American Ecological Engineering Society

Journal of Ecological Engineering Design
jeed.pubpub.org

Supplementary Material

Modeling Phosphorus Retention and Release in Riparian Wetlands Restored on Historically Farmed Land

Adrian R.H. Wiegman[1,2,3], Kristen L. Underwood[2,4], William B. Bowden[1], Isabelle C. Augustin[4], Tiffany L. Chin[1], Eric D. Roy[1,2,4]

[1]Rubenstein School of Environment and Natural Resources, University of Vermont, Burlington, Vermont, USA
[2]Gund Institute for Environment, University of Vermont, Burlington, Vermont, USA
[3]Pasture Systems and Watershed Management Research Unit, USDA-ARS, East Wareham, Massachusetts, USA
[4]Department of Civil and Environmental Engineering, University of Vermont, Burlington, Vermont, USA

Correspondence
Eric D. Roy
Rubenstein School of Environment and Natural Resources
University of Vermont
Burlington, VT 05405, USA
Email: eroy4@uvm.edu

TEXT S1. ADDITIONAL MODEL DOCUMENTATION

A note on terminology

The term dissolved inorganic P (DIP) encompasses various orthophosphates, and polyphosphates, which represent the most mobile, and reactive fraction of phosphorus in the environment (Ruttenberg 2014). Soluble reactive P (SRP) refers to chemical analyses (e.g., molybdate blue colorimetry, Murphy and Riley 1962) that detect orthophosphates (i.e., DIP) as well as acid hydrolysable organic phosphate. DIP comprises the majority of SRP in most cases, and Nürnberg and Peters (1984) found that at least 80% SRP was potentially bioavailable in samples from 13 freshwater lakes. DIP and SRP are often used interchangeably (Jarvie 2002). For the purposes of this paper, we assume DIP is equal to SRP. In the main article of this paper, we exclusively use the term DIP. This is consistent with other modeling studies and textbooks, which tend to split P fractions into functional groupings (e.g., dissolved/particulate, organic/inorganic, labile/recalcitrant) (Wang et al. 2003; Marois and Mitsch 2016; Reddy and DeLaune 2008; Ruttenberg 2014). However, in this Supplementary Material document we use SRP and DIP to distinguish between analytical measurements and the *wetlandP* model, respectively. Here, DIP refers only to *wetlandP* state variables and parameters, and SRP refers only to analytical measurements.

Documentation

A stable version of the *wetlandP* model (version 2.1) that was used in this paper (including detailed documentation, input data, output data, and scripts for implementation, pre/postprocessing) is freely available on GitHub: (https://github.com/arhwiegman/wetlandP_2p1_stable).

Initial model development

Initial development of the *wetlandP* model included defining numerous state variables, flows, and rates. Our primary objective during development was for the model to be able to simulate the key processes influencing net P retention in a riparian wetland during flood inundation events, including P deposition and dissolved P dynamics. Modeling these processes required representation of P transport into and out of the wetland system with floodwater, inorganic P chemistry (sorption/desorption), particle settling, diffusion at the sediment-water interface, transformations of organic P to inorganic P (mineralization), and assimilation of inorganic P into live biomass (immobilization) (Reddy and Delaune 2008). This was accomplished by including aboveground and belowground compartments with biomass, organic, and inorganic P stocks, linked by various flows that could be calibrated based on our field measurements or literature values (see documentation on GitHub and Figure 1 in main article).

The current version of the *wetlandP* model includes subroutines that characterize: (i) relationships between depth and storage volume in the surface water and the active soil layer, (ii) relationships between water level and hydraulic residence time determined using previously developed models and our field measurements (e.g. Box S1), (iii) wetland P concentrations in the surface water and soil, (iv) P mass fluxes into and out of study control volumes, (v) meteorological observations from nearby stations, (vi) water temperatures and dissolved oxygen

concentrations necessary for adjusting P transformation rates, and (vii) plant community characteristics.

Box S1. Hydrology subroutine in the *wetlandP* model.

$$V_w = H_w A_w$$

$$\Delta V_w = V_{w,t} - V_{w,t+1}$$

$$Q_{net} = \Delta V_w - A(ip - ET)$$

$$Q_{net} = Q_{in} - Q_{out}$$

IF $Q_{net} > 0$:

$$Q_{in} = V_w/HRT + Q_{net}$$

$$Q_{out} = V_w/HRT$$

ELSE:

$$Q_{out} = V_w/HRT + Q_{net}$$

$$Q_{in} = V_w/HRT$$

Preliminary testing of the *wetlandP* model included inspection of time series plots for model state variables, visual comparison of state variable values with field observations, confirmation of model mass balance, and evaluation of model performance under increasing complexity of the simulation (see online documentation on GitHub for details).

The *wetlandP* model is integrated on subdaily temporal resolution using the `lsoda` function from the deSolve package, but TP and DIP mass balances were estimated by postprocessing outputs at daily resolution; this produces a small analytical error due to differences in numerical integration. We compared the estimate of TP balance from surface water exchanges with the difference in total P from the sum of P pools in all compartments between the initial and final states of a given simulation. We found that the mean absolute error across all simulations for this method was 1.5% (5th percentile 0.1% and 95th percentile: 5%) and decreased exponentially as net TP balance increased.

Key model assumptions

The *wetlandP* model has sufficient complexity to simulate key processes affecting P retention and release in riparian wetlands using a relatively small number of local parameters for soil, water quality, and hydroclimate. For a complete list of parameters see the online documentation on GitHub.

To allow for the model to simulate a wide range of conditions with relatively few parameters, we designed the model to be relatively simple. We made several assumptions in order simplify the model relative to its predecessors (Hantush et al. 2013; Marois and Mitsch 2016; Wang et al. 2003). Key model assumptions include the following:

1. Groundwater inputs
    a. We only explicitly modeled lateral surface water exchanges in and out of the system and vertical exchanges between the surface water and active soil layer within the wetland because silt rich organic soils typical of riparian wetlands have high water holding capacity (Libohova et al. 2018) and groundwater exchanges typically comprise small fractions of water budgets of riparian wetlands underlain with low-permeability soils (which was the case for our study wetlands) (Lent et al. 1997; Jones et al. 2015).
2. DIP (i.e., SRP) (de)sorption
    a. Ex_max is the variable name used in the Wetland P Model for the maximum storage (i.e., sorption) capacity for exchangeable P in the soil (mg P/kg). Ex_max is noted as P_{max} in Figure 9a of the main article and is also commonly noted at PSC (for P Storage Capacity) in the literature. We assume that the P equivalent of oxalate extractable Al plus Fe represents Ex_max [Ex_max = 31*(Al/27+Fe/56)]. We assume that oxalate extractable P represents the exchangeable inorganic P pool (model variable name = Ex). Ex is noted at 'P' in the 'wetland soil' panel of Figure 9a. Therefore, the product of the Oxalate P Saturation Ratio (PSR, mol/mol) [PSR = (P/31)/(Al/27 + Fe/56)] and Ex_max was used to initialize the particulate inorganic P (PIP) pool in the model's belowground compartment.
    b. Based on our field observations, riparian/floodplain wetland water columns experience intermittent periods of aerobic and anaerobic conditions. We therefore decided to use equilibrium DIP (DIP_E) values in our modeling that were based on the final SRP concentrations observed during the aerobic (O_2) treatments in the laboratory intact core experiments. Those experimental treatments included daily reaeration with subsequent declines in DO, similar to most of our field observations. Langmuir model parameters have been used in past models to simulate equilibrium P dynamics (e.g. Wang et al. 2003). However, we found poor correlation between Langmuir model parameters and SRP fluxes in our laboratory intact core experiments.
3. Inorganic soil accretion (settling, outflows)
    a. There is no significant bioturbation effect.
    b. Adsorption occurs only below the soil surface and does not occur in the water column.
    c. Inflow concentrations of inorganic sediments, as well as dissolved and particulate inorganic P, are derived from median stream concentrations of TSS and TP unless otherwise noted.
4. Organic soil accretion (growth/decay, inflows)
    a. There is one generalized type of primary producer that synthesizes aboveground and belowground biomass in equal proportion, but with differing

turnover rates. Aboveground biomass turns over at least once per year with winter senescence, while belowground biomass can take many years to turnover.

b. Tissue concentrations of P are the same across all forms of organic matter, live biomass, or litter, including labile and refractory organic matter.
c. The decomposition rate coefficient of labile organic matter is affected only by temperature. Refractory organic matter, which represents lignin-rich material (phenolic compounds; Morris et al. 2016), does not decompose when the wetland is inundated (Freeman et al. 2001). However, when water falls below the wetland surface, refractory organic matter decomposes in the same fashion as labile organic matter, but with a much lower rate coefficient.
d. Inflow concentrations of labile and refractory organic sediments and P are derived from median stream/inflow concentrations of TSS and TP, thus, to not vary in time or with flooding depth.

5. Periphyton, phytoplankton, and dissolved oxygen dynamics are not currently represented in the *wetlandP* model.
    a. Periphyton uptake of DIP from surface water during warm periods could potentially limit DIP movement from soils into surface water during inundation events (Dodds 2003). Phytoplankton could also assimilate DIP in surface water and alter P dynamics (Wang & Mitsch 2000; Trentman et al. 2020). On the other hand, oxygen depletion of surface waters could promote higher equilibrium DIP concentrations due to dissolution of Fe and associated P (as seen in our intact core incubations) (Wiegman et al. 2022). In our model here, we used equilibrium DIP concentrations derived from aerobic incubations with diurnal fluctuation in surface water dissolved oxygen (Wiegman et al. 2022). At present it is not clear which mechanisms have a greater effect on simulated net TP and DIP balances. Future versions of the model could incorporate periphyton, phytoplankton, and dissolved oxygen dynamics and evaluate their relative importance for net TP retention and net DIP retention.

Model calibration and scenarios: Overview

Model input parameters fall into three groups: (A) local (measured) parameters, (B) stochastic (unmeasured) parameters, and (C) universal parameters. Universal parameters are precisely known, and do not vary within the model scope (e.g., the viscosity of freshwater water at 20ºC, the particle density of inorganic sediments). The values for universal parameters were taken directly from literature values. The distinction between local and stochastic parameters is the feasibility of their measurement/derivation. Local parameters vary from site to site and are feasibly measured or derived across many sites. These include parameters that define the initial conditions of state variables (soil, water, vegetation), hydrologic flows, and inflow concentrations. The values for local parameters were taken from field/lab measurements from this study. Stochastic parameters may or may not vary from site to site but are impractical to measure at a wide number of potential wetland restoration sites (many thousands have been identified in Vermont). Stochastic parameters in the model tend to be rate coefficients that affect process flows (e.g., the rate of decay of plant litter) or partitioning coefficients that relate the size of one pool to the size of another (e.g.,

the labile fraction of decomposing litter). The initial range values for stochastic variables were informed by the literature, then were calibrated to our field and lab data. We evaluated the impact on model parameters on TP retention using global sensitivity analysis using a steady state simulation (forcing variables constant over time).

For calibration, verification, and sensitivity analysis, we executed the model using data between 7/15/19 and 7/15/21 for sampling plots 0, 2, and 4 at each site. We used year 1 data for model calibration. The model was verified with field data from year 2 using the three criteria outlined in the main article, except for accretion P (data unavailable for year 2). Both years of data were used to evaluate various scenarios for a sensitivity analysis.

Data preprocessing was required prior to model execution. We set the dry mass and P stocks of biomass (aboveground shoots and belowground roots), and soil to the mean values from samples collected in summer of 2019. We assumed that equilibrium DIP parameter (DIP_E) was equal to the final DIP concentration from aerobic intact core experiments including diurnal fluctuation in surface water dissolved oxygen (Wiegman et al. 2022). We estimated inflow concentrations of various P stocks from median values of TSS (mg L^{-1}), TP (mg P L^{-1}), the organic fraction of TSS (mg mg^{-1}), and the DIP fraction of TP (mg P mg P^{-1}).

We preprocessed the hydroclimatic data for each site and plot based on measured water levels and data from local meteorological stations. For sensitivity analysis and scenarios, identification of feasible ranges in hydrologic variables at the two Otter Creek sites (Union St and Swamp Rd) was informed by a review of existing models for the region, including a 2D HEC-RAS model for the Otter Creek (Trueheart et al. 2020). At Prindle Rd, we used field measurements (including at the system outlet) to estimate the relationship between hydraulic retention time and water level throughout the study.

Preprocessed model inputs included water elevation and temperature recorded by HOBO MX2001 pressure sensors at 10-minute intervals, and sub-hourly meteorological data from the BTV Airport (NOAA NCDC) used to estimate precipitation and evapotranspiration. The HOBO data were summarized to daily values by taking the average temperature, and the maximum water height each for each calendar date in the record, then converted to estimates of water height and storage volume (m^3/m^2) for each plot. The meteorological data were summarized to daily values by averaging temperature, cloud cover, windspeed, and relative humidity, and by summing precipitation totals. Evapotranspiration rates were estimated with the Penman-Monteith method using cloud cover, temperature, relative humidity, and windspeed (r `evapotranspiration` package). Net surface flow (inflow/outflow) was estimated by adjusting changes in water volume for estimated precipitation and evapotranspiration. Inflow and outflow were deduced from net surface flow by adding a term for throughflow, which was calculated as the water volume divided by hydraulic residence time (Box S1). Hydraulic residence time was modeled as a function of elevation relative to the lowest elevation sampling plot according to a negative power law relationship that was calibrated to each site.

We ran all scenarios over the two-year monitoring period using our calibrated model with inflow concentrations derived from (a) siphon data collected at sampling plots or (b) grab samples

collected in the inflow/river. The simulations where inflow concentrations are derived using siphon data included the default parameters and used data from median estimates from passive siphons as inflow TSS and P concentrations to sampling plots. The siphon simulations were used for calibration and verification but do not necessarily provide a representative estimate of how the whole system is functioning. For example, sediments can be deposited and dissolved P may flux out of soils as river/stream water passes through the wetland on its way to each sampling plot. Simulations using median concentrations from the grab samples collected at river/stream inflow locations provide a more representative estimate of the ecosystem level TP retention, therefore only these simulations are given when we report net TP retention estimates in the results of the main article.

Model calibration and scenarios: Details

Calibration to intact cores

Stochastic parameters that affect adsorption and diffusion were calibrated by simulating a 2-week incubation of cylindrical (7.6 cm diameter) intact soil cores that were maintained at a water depth (Hw) of 0.2 (m). Surface area (A) was set to 0.0181 (m^2, calculated from diameter, pi*(diameter/2)^2), and volume of the water column aboveground (Vw) was set to 0.00362 (m^3, calculated as A*Hw). The hydroclimatic forcing variables were the same for each intact core except for temperature (which was set to the mean of the incubation). Precipitation (Q_precip) and net infiltration of groundwater (Q_ground) were set to zero, surface outflow (Q_out) was set equal to 5e-6 (m^3, 5ml daily water samples collected from each core), surface inflow (Q_in) was set to the 7e-6 (m^3, set equal to the average daily volume added across all cores of 7ml), and Q_ET was set to the difference between Q_in and Q_out. All model processes were simulated during this experiment except assimilation of inorganic P by biomass. Biomass and litter stocks were set equal to zero. Input concentrations of TSS were set equal to zero, and the soluble-reactive fraction of TP was set to 1.

The local (measured) parameters that were varied by site were organic matter content of the soil (k_LOI, g/g, soil loss-on-ignition), the maximum P storage capacity of a soil (k_Ex_max, g P/kg, 31*[Ox-Al/27+Ox-Fe/56]), the initial ratio of particulate inorganic P (PIP) to the maximum P storage capacity (k_PSR, mol/mol, oxalate P saturation ratio = [Ox-P/31]/[Ox-Al/27+Ox-Fe/56]), and the initial inflow concentration of TP (k_TP, equal to the initial SRP concentration of filtered site water). The stochastic parameters that affect adsorption and diffusion are the adsorption bond strength coefficient (k_E), adsorption rate coefficient (k_ad), and effective diffusion rate coefficient (k_diff). We first estimated the value of k_E, by minimizing the sum of squared residuals to the calculated equilibrium DIP concentration (DIP_E = k_Ex_max*k_PSR/(1-k_PSR*k_Ex_max)*k_E) and final SRP value observed in intact cores. Next, we adjusted the values of the k_ad and k_diff so that the shape of the DIP vs time curve in model simulations lined up reasonably well with observed data and recorded a range of plausible values.

Calibration to field data

To calibrate/verify the model against data measured in the field, we simulated monitoring plots (15 total) of three wetland ecosystems sites for one wet season from October 1, 2019 to July 15,

2020. Like in the simulation of intact cores k_LOI, k_Ex_max, and k_PSR, were used as local parameters to initialize the belowground compartment. In addition, TSS (k_TSS, g/m^3=mg/L) and TP (k_TP, g/m^3), the organic fraction of TSS (k_f_OSS, g/g), and the soluble-reactive fraction of TP (k_f_SRP, g/g) were used as local parameters and for conversions to the various stocks represented in the model (IM, OM, PIP, LOP, ROP, and DIP) using three stochastic parameters (k_SRP2LOP, k_ISS2PIP, k_OSS2ROP) that were fit to data collected from all three sites. The values for k_TP, k_TSS, k_f_OSS and k_f_SRP were set equal to the median value observed at inflow monitoring locations of each site. At Prindle Road, we used data from the northern and eastern culverts. At Swamp Road, we used data from the bridge and the southern ditch (DS). At Union Street, we used data from the bridge, the ditch plug (DP), and the second culvert east of the bridge (C2) (see site maps in Figure 1 of main article).

Inorganic accretion is affected by in large part by hydroclimatic forcing variables and the following local (measured) parameters: hydraulic residence time (k_HRT), the influent concentration of TSS (k_TSS) and TP (k_TP), the organic fraction of TSS (k_f_OSS), and soluble-reactive fraction of TP (k_f_SRP). Once inorganic accretion rates were adequately reproduced by the model (Figure S1), we calibrated assimilation and decomposition parameters to the stocks of litter P observed in the wetlands during litter bag decomposition experiments. Organic matter accumulation accretion rates are sensitive to assimilation, mortality, hydrologic inflow rates, and inflow concentrations. Stochastic parameters that affect organic accretion are the annual rate of net primary productivity (k_NPP, $g/m^2/yr$), the mortality rate of live biomass (k_M, g/g), the P content of biomass and all forms of organic matter (k_BM2P, g P/g dw), the labile fraction of OM/P (k_f_labile, g/g), and the decomposition rates of litterM/P (k_decay_litter, g/g), LOM/P (k_decay_LOP, g/g), and ROM/P (k_decay_ROP, g/g). The plausible range for parameter values was first informed by the literature (see Appendix A). Then we manually estimated values of k_M and k_NPP that yielded stable stocks of below ground biomass between 1000 and 2000 g dw m^{-2} while also yielding peak aboveground biomass values of 400-800 g dw m^{-2}, approximate averages observed at our three field sites (Figure S2). Then we adjusted litter decomposition rates until litter P fell within the range of field observations of stocks (Figure S3). Once biomass and litter were in line, we checked that soil organic matter content was not increasing by more than 2% per year, and repeated the process as needed until all calibration criteria were met. Figures S1, S2, and S3 below show results from this process.

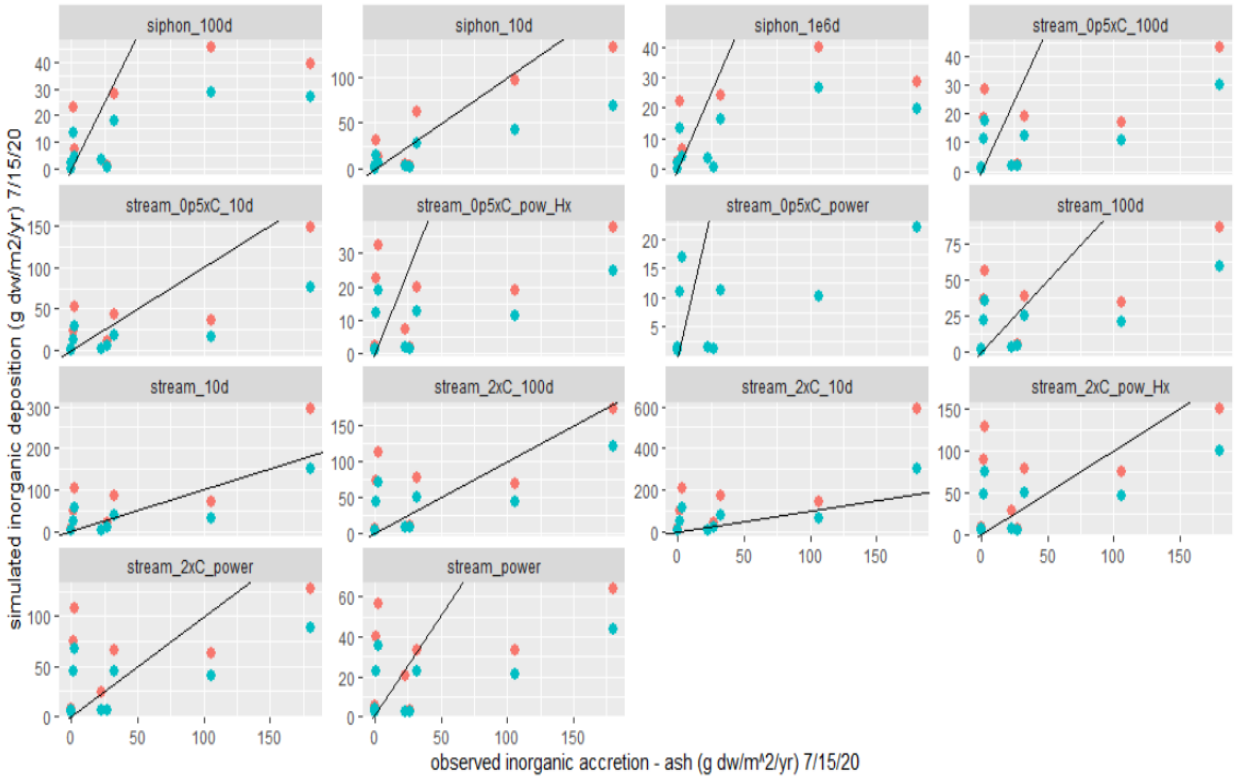

Figure S1. Observed versus simulated change in inorganic matter for plots 0, 2, and 4 for a range of concentration, HRT assumptions, and particle trapping assumptions. Siphon = median siphon concentrations at each plot, stream = median stream concentrations, 0p5xC = 0.5 x stream median concentration, 2xC = 2 x stream concentration, power = power model of HRT, 10d = 10-day HRT, 100d = 100-day HRT. Red/pink points = 100% particle trapping, blue points = modeled particle trapping.

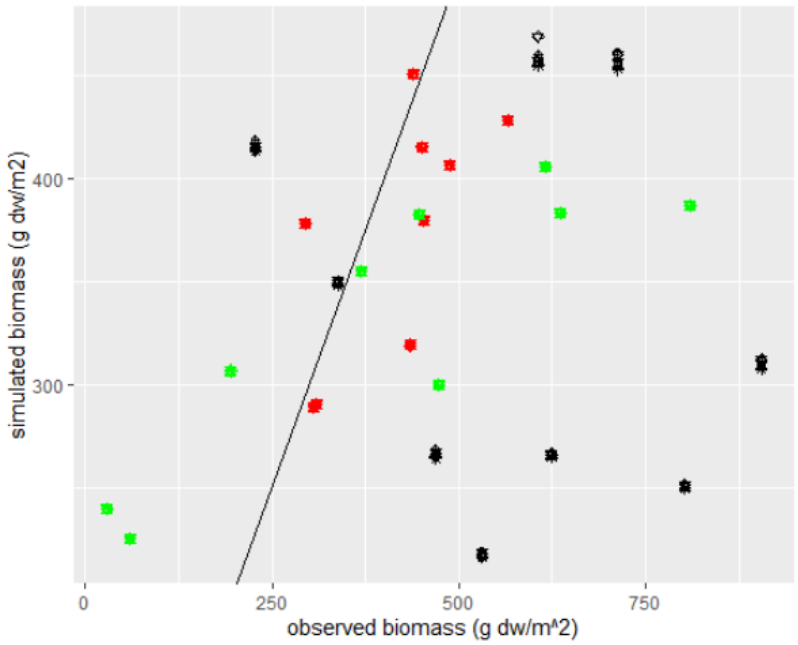

Figure S2. Simulated vs observed biomass for plots 0, 2, and 4 at all sites. Red points are biomass stocks observed on 9/02/19, green points are biomass + fresh litter collected on 10/15/19, and black points are biomass and fresh litter observed on 10/15/20. The black line is the 1:1 line.

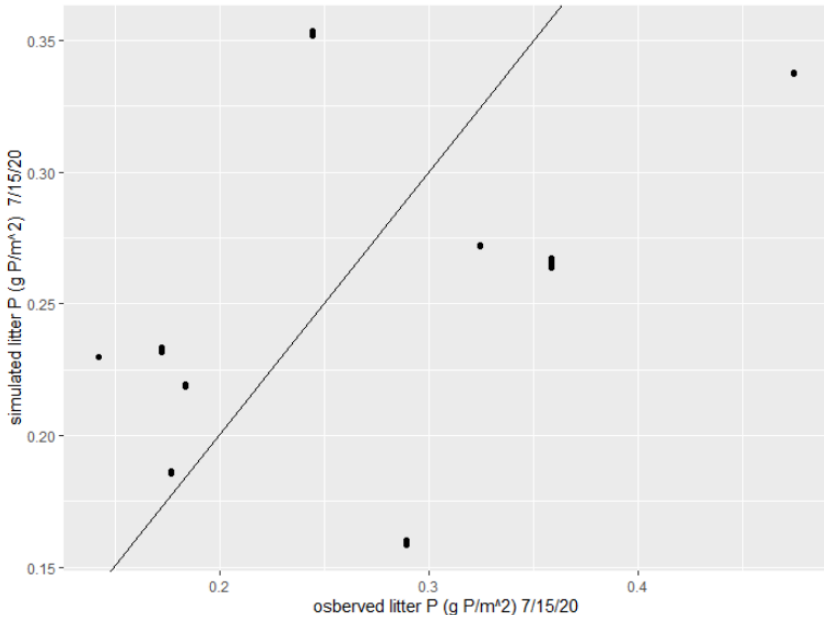

Figure S3. Observed verses modeled stock of litter P 7/15/20 for plots 0, 2, and 4 at all sites. The black line is the 1:1 line.

Inflow concentrations

Inflow concentrations affect many processes that influence P balance, including sedimentation, adsorption, and diffusion. We used TSS, the organic fraction of TSS (k_f_OSS), TP, and the soluble reactive fraction of TP (k_f_SRP) as input parameters to the model, then converted these into various mass stocks represented in the model: IM (mass of inorganic sediments, g), OM (mass of organic sediments, g), PIP, LOP, ROP, DIP. We assumed that IM was equal to ISS=TSS*(1-k_f_ISS), and that DIP was equal to SRP=TP*k_f_SRP. We calculated observed non-SRP as the difference between TP and SRP and assumed that non-SRP was the sum of PIP, LOP and ROP. We assumed that ROP and LOP scaled proportionately to OSS, PIP scaled proportionately in part with ISS and in part with SRP. We calculated LOM and ROM based on estimated LOP and ROP concentrations, and k_BM2P (the P content of biomass) and k_f_labile (the labile fraction of live biomass), and OM as the sum of LOM and ROM. Each of LOP, ROP, and PIP, were calculated using a scaling coefficient to convert SRP to PIP (k_SRP2PIP), ISS to PIP (k_ISS2PIP), and OSS to OP (k_OSS2OP). We set k_OSS2OP equal to 0.001 (g P/g dw) the value used for the P content of organic matter and live biomass (k_BM2P). Then, we solved for the values of k_ISS2PIP and k_SRP2LOP at each site by minimizing the sum of squared errors between the observed non-SRP (TP-SRP) and modeled non-SRP (k_ISS2PIP*ISS + k_OSS2OP*OSS + k_SRP2PIP*SRP) using the GRG nonlinear optimization method from the `solver` add-in in Microsoft Excel. Figures S4 and S5 show the observed verses fitted data with various approaches to estimate the parameter values. For the simulations in the scenario analysis, we used Local & Global fit (Figure S4b and S5). For simulation of a hypothetical system within the Vermont portion of Lake Champlain Basin, we recommend using the All Global Fit (Figure S4c).

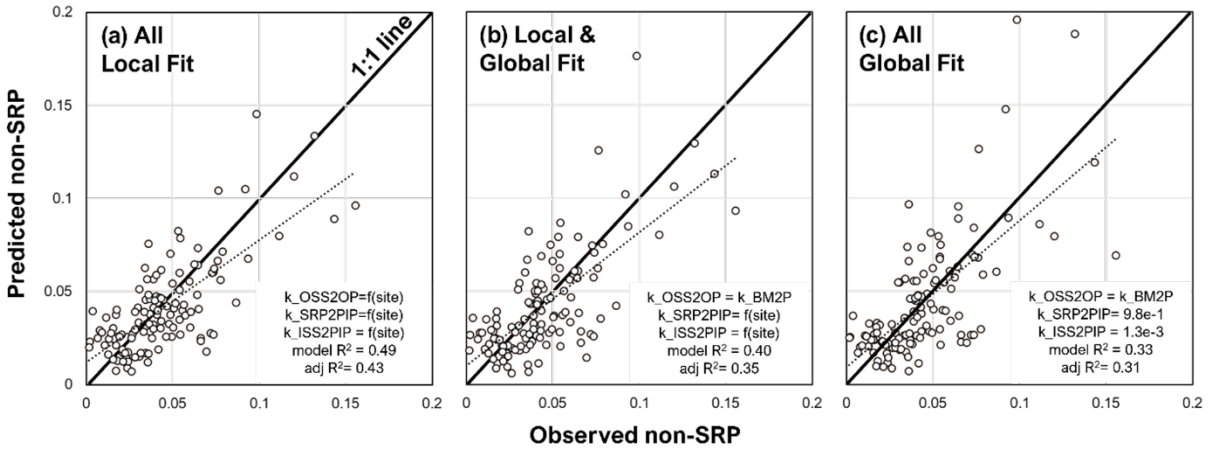

Figure S4. Observed vs predicted non-SRP concentrations using local (a, k=9), partial (b, k=6), and global (c, k=3) parameter estimates (n=131).

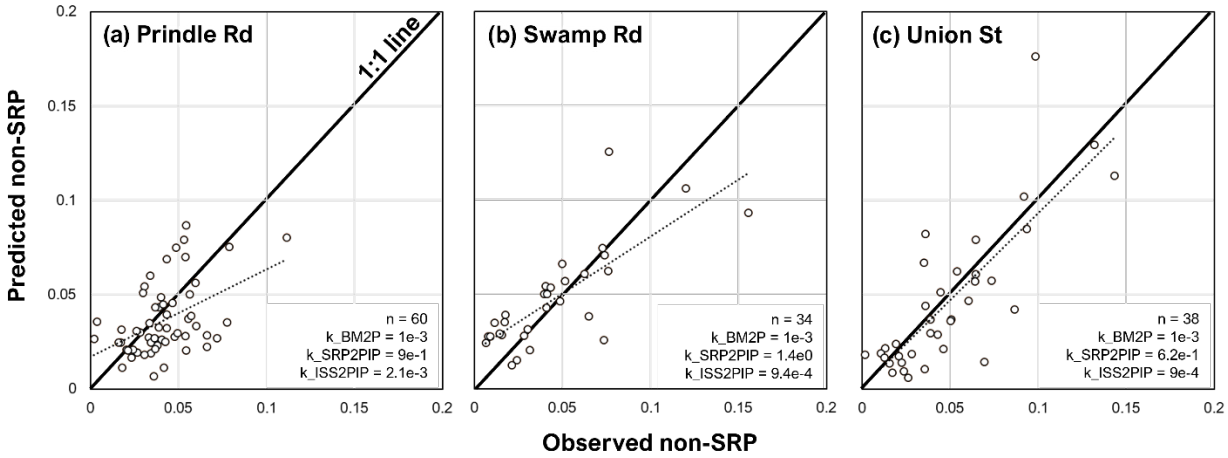

Figure S5. Observed vs predicted non-SRP (TP – SRP, mg P/L) and estimates of scaling coefficients convert SRP to LOP (k_SRP2LOP), ISS to PIP (k_ISS2PIP), at Prindle Rd (a), Swamp Rd (b) and Union St (c). The 1:1 line is the thick black line. Dotted line shows the regression on observed (x) vs predicted (y).

Hydraulic residence time

Hydraulic retention time or residence time is the measure of the average amount of time a molecule of water will spend in a control volume before leaving. HRT is calculated by dividing the system volume by the volumetric outflow rate. At Prindle Road, this was achieved by creating a relationship with water height (measured continuously) and storage volume and collecting multiple outflow velocity measurements over the course of monitoring (Figure S6). We converted outflow velocity measurements to volumetric flow rates (discharge) by multiplying velocity by cross sectional area. To estimate cross sectional area as a function of water level at the outflow, we set up a level line then measured the height of the water level sensor below the level line and measured the height of the channel bottom at 30cm intervals across the width of the floodplain. We fit a regression between discharge and stage (water level) to estimate discharge as stage varied over time, and then interpolated estimates of storage from LiDAR using the ArcGIS Storage Capacity tool.

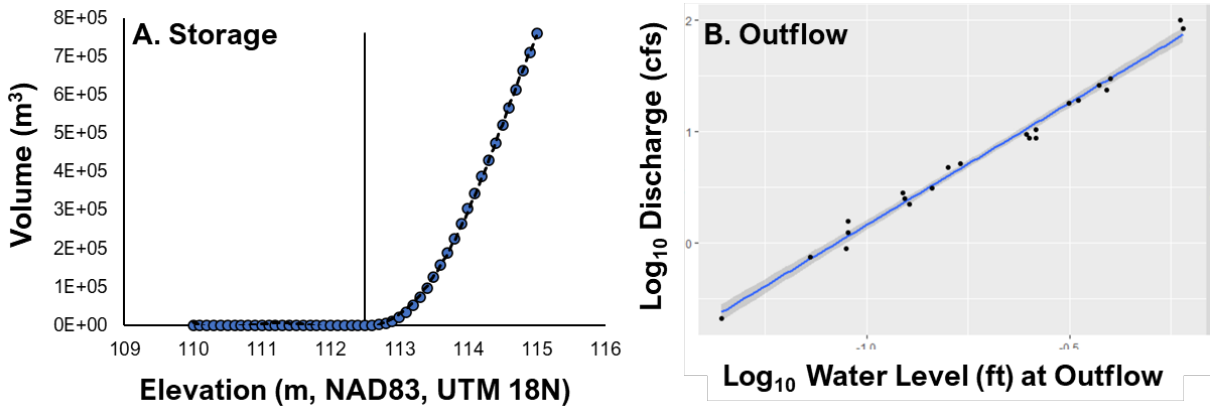

Figure S6. Relationships observed between elevation/stage (continuously logged by HOBO MX2100), storage volume estimated from LiDAR (A) and outflow (B). The black vertical line on A shows the elevation of the water level logger in the wetland. Water levels were continuously logged, while discharge calculated from velocity and cross-sectional measurements at outflows.

At Otter Creek sites, we estimated the general magnitude of HRT in the floodplains using two HEC-RAS simulated floods, May 2019 and April 2018. We did this by exporting raster grids of the depth and velocity (magnitude) for the entire model domain at the time of peak flow at Union Street and Swamp Road bridges. This resulted in raster grids exported at four times (Table S1).

Table S1. Date, time, location of peak discharge of Otter Creek HEC-RAS simulated flood peaks.

Date and time	Location of Peak	Discharge at Peak
2018-05-01 09:40	Union St	96.9 m^3/s (3420 cfs)
2018-05-03 18:20	Swamp Rd	89.6 m^3/s (3160 cfs)
2019-04-16 16:40	Union St	254.6 m^3/s (8990 cfs)
2019-04-18 06:00	Swamp Rd	168.2 m^3/s (5940 cfs)

We digitized a polygon of the river and of the entire floodplain between the monitoring bridge and the next constraining feature downstream (in both cases another bridge) (Figure S7). We clipped each raster to the extent of the channel only, the floodplain only, and the floodplain and the channel and calculated the volume of water held in each extent. We then extracted depth and velocity values across the upstream boundary transect. For each cell along the transect, we calculated cross sectional area (depth * width) and discharge (area * velocity). We then summed the discharge for the channel only, floodplain only, and floodplain and channel. We calculated HRT by dividing the volume by the discharge estimated for the channel only, floodplain only, and both channel and floodplain.

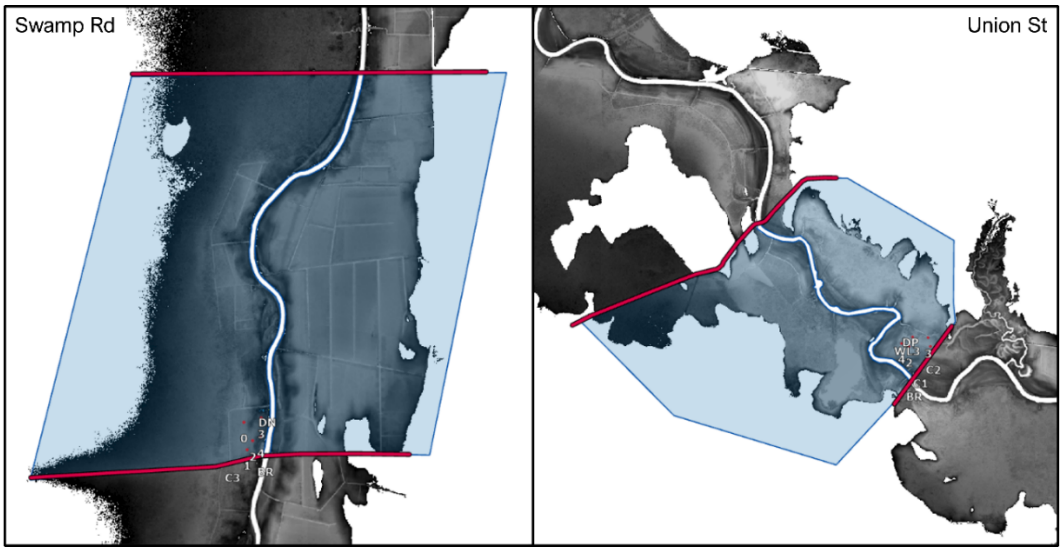

Figure S7. Depth of inundation in otter creek showing location of sampling plots and the reach polygons (blue shaded areas) used to calculated system storage volume, and cross sections (red) were velocity and cross-sectional area were used to estimate discharge through the floodplain.

HRT followed a negative power law with discharge and depth of flooding at all three sites (Figure S8). Swamp Road had the highest residence time of the three sites. Prindle Road and Union Street had similar relationships between water level and residence time, but Union St had relatively greater residence at water levels above 0.6m than Prindle Rd. At all sites, HRT was above 10d when water levels were below 0.5m, suggesting that below this point flow was governed predominantly by changes in volume (floodplain filling and draining) rather than throughput.

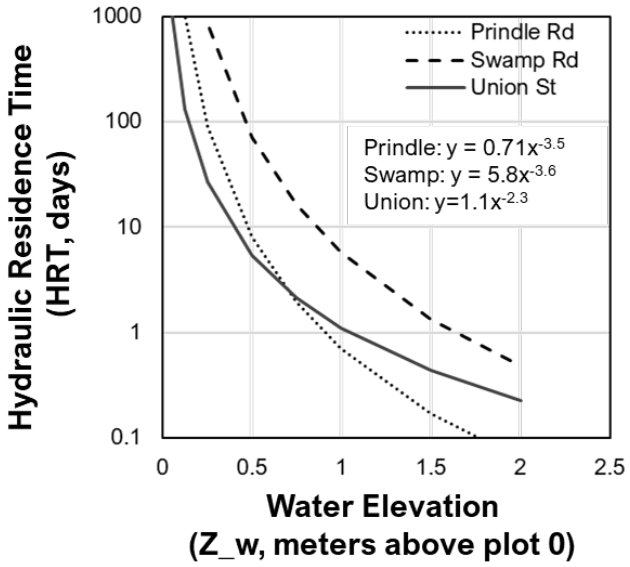

Figure S8 Power model of Hydraulic Residence Time (HRT), as a function of Water Elevation relative to the lowest elevation plot in the wetland. The parameters for each site were generated from data points extracted for system wide volume and discharge at various flood stages.

Sensitivity analysis

We used a steady state model with the calibrated default parameters to investigate model sensitivity to four tests that examined changes in the following:

(1) **Local water quality:** Randomly varying inflow TSS and P concentrations and initial state variables while holding hydroclimatic variables and stochastic parameters constant.
(2) **Local hydrology:** Randomly varying hydroclimatic variables while holding inflow TSS and P concentrations and initial state variables and stochastic parameters constant.
(3) **All local parameters:** Randomly varying all local parameters (concentrations, states, hydroclimatic variables) while holding stochastic parameters constant.
(4) **Stochastic parameters:** Randomly varying stochastic parameters while holding all local parameters constant.

We did this by employing the Global Sensitivity Analysis technique (Haan 2002). Briefly, we conducted 10,000 Monte Carlo simulations for each sensitivity test described above, with randomly generated values for each parameter varied in the test. Random values were drawn from either a log-normal or uniform probability distribution. To ensure reproducibility, we called the `set.seed` function with a value of 1 prior to generating the parameter values. For each simulation, we extracted the initial value of the state variables and calculated the difference and percent difference in state variables between the first and last time point. The extracted data was stored in a data table containing random values for each parameter, the name of the sensitivity test and the simulation number (1 to 10,000). To measure the relative effect that each parameter

had on the model for each sensitivity test, we produced a correlation matrix between the input parameters and outputs. We computed both Pearson product moment correlation coefficient and Spearman's rank correlation coefficient (Hantush et al. 2013). The Spearman coefficient indicates the strength of a monotonic relationship (linear or nonlinear), while the Pearson coefficient indicates the strength of a linear relationship. A large difference between the Pearson and Spearman coefficients indicates nonlinearity.

Using Global Sensitivity Analysis allowed us to examine the effects of parameters on net TP balance. We used these results to determine whether the model was performing as we thought it should be based on our understanding of biogeochemistry, and to assess the magnitude and direction of impacts that changes in local site conditions have on net TP retention. Figures S8, S9, and S10 show the correlation strengths of the parameters in the suite of sensitivity tests we conducted. When local concentrations were varied and hydroclimatic parameters and stochastic variables were fixed, we found that k_Ex_max, k_PSR, and k_LOI had significant negative Spearman correlation with net TP balance, indicating that increases in these variables were associated with greater TP loss from the wetland (Figure S9). When varying all local parameters simultaneously, we found that the correlation strengths for k_TP and k_f_SRP were of similar magnitude to k_Ex_max and k_PSR (Figure S10), with the former having increased in correlation strength from when only concentrations were varied, while the latter decreased in correlation strength. When holding local parameters constant and varying all stochastic parameters, we found that k_E had by far the greatest impact on net TP balance, with a Spearman correlation ~0.7 and a Pearson correlation near ~0.3, indicating nonlinearity (Figure S11).

Model scenarios altering HRT or water levels provide insights into how system hydrology affects net P retention. Such changes could potentially occur because of restoration actions that alter site hydrology, changes in land management that affect peak flows, year to year variability in precipitation patterns, or climate change. Scenario testing used to investigate biogeochemical control on wetland P retention included running model simulations using different inflow sediment and phosphorus concentrations. Such differences could in reality be driven by upstream land management (e.g., P load reductions resulting from agricultural best management practices) or wetland landscape position.

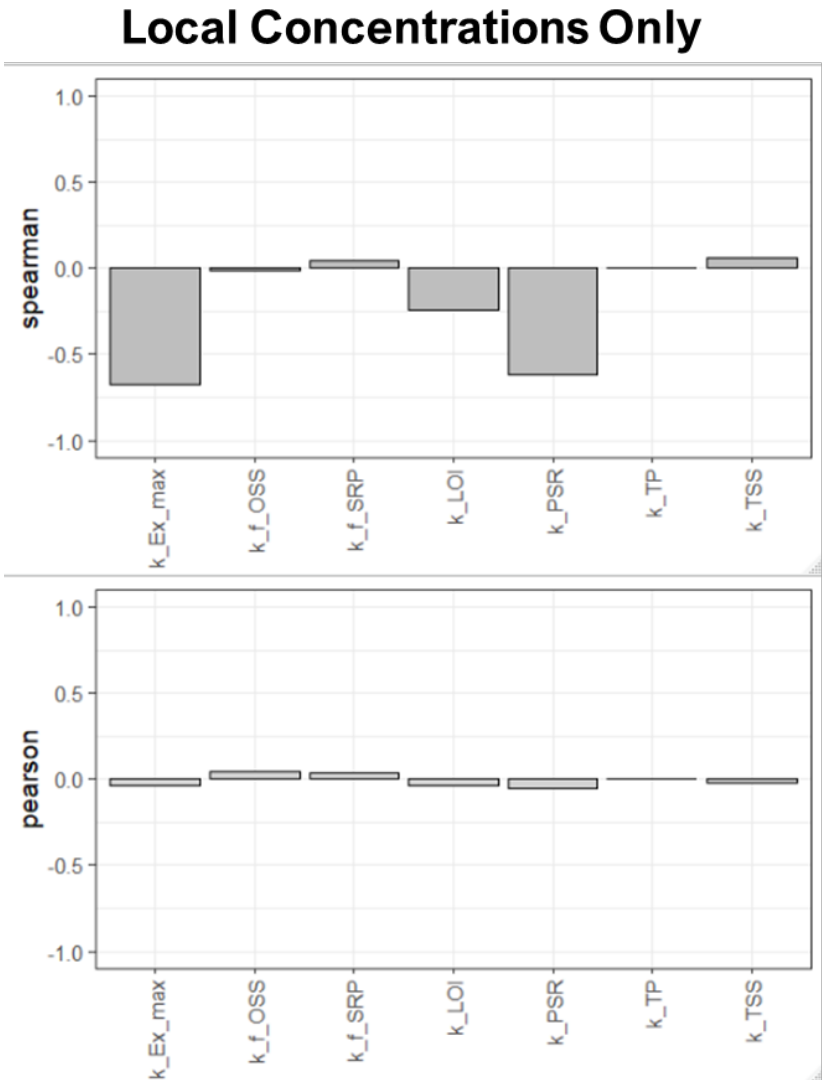

Figure S9. Global sensitivity analysis on net TP balance showing Spearman (top) and Pearson (bottom) correlation for the varying local concentrations only.

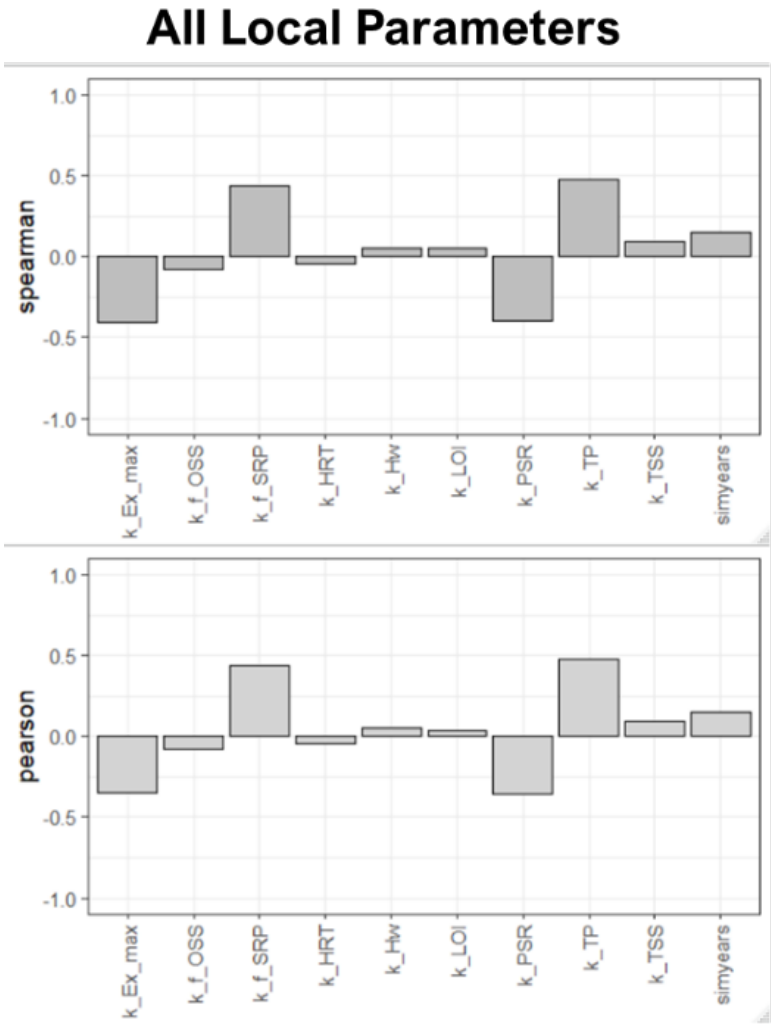

Figure S10. Global sensitivity analysis net TP balance showing Spearman (top) and Pearson (bottom) correlation for the varying all local parameters.

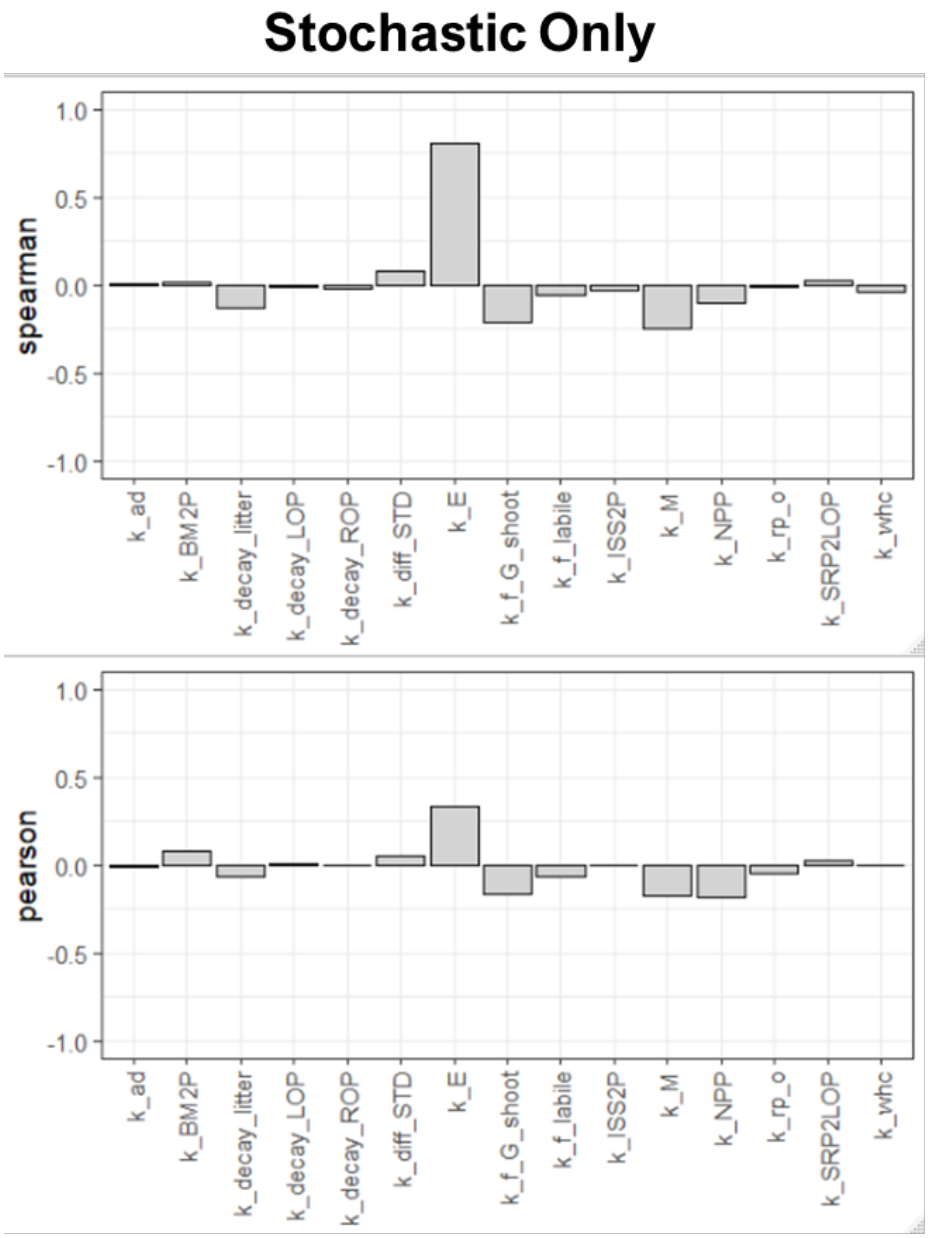

Figure S11. Global sensitivity analysis net TP balance showing Spearman (top) and Pearson (bottom) correlation for the varying all stochastic parameters.

TEXT S2. ADDITIONAL FIELD STUDY DOCUMENTATION

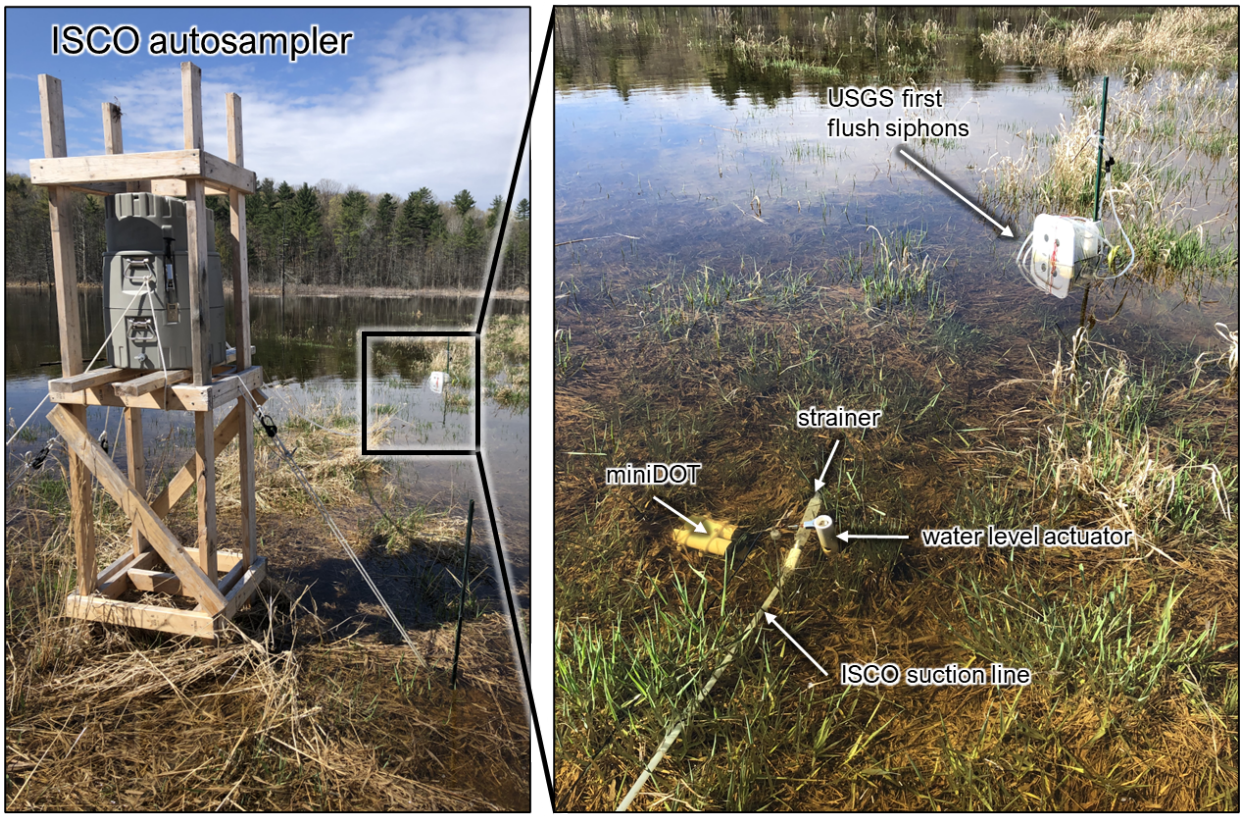

Photograph of water monitoring equipment during a flood at Prindle Rd.

Field and laboratory methods

Study areas

We delineated a sampling zone boundary within an area of each site that had uniform prior land use and perennial emergent vegetation based on available areal imagery in Google Earth Pro (imagery dates: 1995, 2003, 2006, 2008, 2009, 2011, 2012, 2015, and 2016). We then removed areas from each sampling zone that were not likely to receive floodwater at least once during the 2-yr monitoring campaign. At the two Otter Creek sites, the sampling zone was clipped with a polygon of the maximum inundation extent for the spring flood of 2018 (which was a ~Q1.5-year flood). This polygon was produced by a 2D HEC-RAS model (Trueheart et al. 2020) of the Otter Creek floodplain between Rutland and Middlebury and was verified in the field in 2018 by examining the predicted flooding depth against the high-water mark on trees. At Prindle Road, we did not have a model to estimate the maximum flooding extent, so we collected GPS points of the flooding extent during the spring flood in May of 2019, and adjusted the sampling zone not to exceed the elevation of the high-water mark.

We distributed 5 circular plots (5m radius) within each sampling zone along an elevation gradient based on 0.7m resolution LiDAR elevation data (VGCI 2018). This was done by reclassifying the sampling zone at each site into five equal area pentile groups based on elevation, with each group

accounting for 20 percent of the area inside the sampling zone. One sampling plot was randomly placed within each pentile. We also set up additional sampling plots for taking water samples from the river upstream of each site and at ditches and other likely water flow paths during flooding and draining.

Flood monitoring

To monitor surface water stages, we placed water level recorders at high and low elevation plots of each site (OnSET HOBO MX2001-04). At the median elevation plot of each site, we placed optical dissolved oxygen and temperature loggers (PME: miniDOT) equipped with anti-fouling plates and an automated lens wiper (PME: miniWiper).

The median elevation plot of each site had one ISCO autosampler (Model 6712, Teledyne Technologies, Inc.) that collected discrete water samples during the first 24-hr of inundation. ISCOs were programmed to collect surface water samples hourly over 24-hr after water levels exceeded 10 cm above the soil surface. Each wetland sampling plot also hosted replicate USGS-designed first flush (passive siphon) samplers that collected surface water samples 10 cm above the soil surface upon inundation (Diehl 2008). To capture water quality dynamics across the sites over the duration of a flood, 1 L grab samples were collected from the river/stream and inflow and outflow channels at each site, as well as at all inundated wetland plots (up to 5 per site) on the rising and falling limbs of flood events.

The water level recorders were housed inside vented PVC pipes and installed into the ground as shallow groundwater wells. The water level recorders had two pressure transducers separated by 5ft, which allowed for real time local correction for changes in atmospheric pressure. One pressure transducer was kept aboveground at the high elevation plot of each site and was used to calculate water levels if the water depth above the low elevation recorder exceeded 5 ft.

The ISCOs were placed outside the perimeter of the sampling plot and were fastened 1.5 m above the sediment surface to a wooden frame. Each ISCO had a 25 ft suction-line and strainer that was held at 10 cm above the sediment surface at the center of the sampling plot. An actuator triggered sampling when water levels rose above the strainer (Model 1640, Teledyne Technologies, Inc.).

The siphon samplers (Diehl 2008) consisted of a 1 L narrow mouth amber Nalgene bottle sealed at the top with a no. 7 two-hole rubber stopper. The stopper held a siphon made from copper tubing, and a vent tube made from vinyl tubing that enabled water flow into the bottle after water levels rose above the crest of the copper tubing. Duplicate siphons were fixed sideways attached to a pole at each plot center and were positioned to trigger when water exceeded 10cm above the sediment.

To collect grab samples, wide mouth 1 L amber Nalgene bottles were attached to an extendable pole fitted with hose clamps. Each YSI parameter was calibrated daily before each sampling trip and verified with a reference solution. During the three flood pulses that were captured by ISCOs, the sites were monitored daily during the rising limb of floods or until ISCO programs had finished, enabling collection of each sample within the U.S. EPA recommended maximum hold time for SRP of 24-hrs (O'Dell 1993).

All water samples were stored on ice during transport and processed immediately at the University of Vermont Aiken Forestry Sciences Lab. Subsamples of 5 mL volume were filtered (0.45 μm) and frozen until analysis for SRP, while subsamples of 20 mL volume were pipetted into pre-cleaned

(acid washed, and 3x rinsed with DDI H_2O) 60 mL borosilicate glass digestion vials and stored in the dark at room temperature for digestion and analysis of total P (TP). The remaining water samples were analyzed for total suspended solids (TSS), as well as mineral (ISS) and organic (OSS) fractions of TSS based on ignition at 550°C (Roy et al. 2016). SRP was analyzed at 660 nm using a microplate reader (BioTek Synergy HT) following the malachite green method for colorimetric orthophosphate analysis (D'Angelo et al. 2001; Ringuet et al. 2011). TP samples were digested following the alkaline persulfate digestion (Patton & Kryskalla 2003) and analyzed using colorimetric orthophosphate analysis at 880 nm on a Lachat QuickChem 8500 using the ascorbic acid method for molybdenum blue (Murphy & Riley 1962).

Vegetation biomass

In early September 2019, aboveground biomass of herbaceous plants (macrophytes) was collected from triplicate 0.5 m x 0.5 m quadrats by clipping vegetation 1-2 cm above the soil or water surface (Dunne et al. 2007). At the same time, belowground biomass was collected in each herbaceous sampling quadrat by collecting the top 10cm of soil with a 7-cm diameter core tube. Biomass samples were placed in a cooler for transport and stored at 4°C until processing, which occurred within 1 month of sample collection. Belowground biomass samples were wet sieved with tap water through a 1mm mesh to remove soil from roots and then dried at 60°C until constant weight (Dunne et al. 2007). In July 2021, diameter at breast height and at 30 cm was measured for trees and shrubs respectively, if woody biomass was present in a plot, then TP stocks were estimated non-destructively using literature values for P content and allometric equations. Aboveground herbaceous biomass samples were clipped into 10 cm pieces dried and weighed to determine dry mass per unit area (g m^{-2}). Herbaceous plant biomass was analyzed for LOI and 1 M HCl-TP using methods described above for soil. TP content for woody biomass was estimated to be 750 mg kg^{-1} based on literature values (Bedford et al. 1999; Cronk & Fennessy 2001).

Litterfall and litter decomposition

Each winter herbaceous plant (macrophyte) biomass senesces and is folded over the soil by snow and ice, so the stock of end-of-season standing herbaceous biomass plus fresh herbaceous plant litter (e.g., dead shoots already fallen) is approximately equal to litterfall production for that year. Aboveground herbaceous biomass and freshly deposited litter was collected in triplicate at each plot from 0.5 m^2 quadrats by clipping standing herbaceous biomass to within 1 cm of the soil surface then collecting freshly deposited litter within each quadrat in October of 2019 and 2020 (prior to flooding). Litterfall was transported, stored, dried, weighed and homogenized in the same fashion as aboveground biomass. Litter mass decay and net P mineralization were estimated using a litterbag decomposition experiment. Briefly, litterbags were constructed from fiberglass window screen (20 cm × 20 cm; 2-mm mesh) and stainless-steel staples. Bags were filled with 10-20g of dry clipped and homogenized litter and labeled with the site, plot, time increment and replicate. In late fall of 2019, five groups of triplicate litterbags were placed at each sampling plot by fastening each to the soil surface with stainless steel 15 cm landscaping staples. Litterbags were retrieved in triplicate after incubating for periods of 0, ~100, ~150, ~250, and ~365 days (Chimney & Pietro 2006). Retrieved litter samples were dried at 60°C for 72 hrs and weighed to determine mass loss and analyzed for organic content and total P using the LOI and 1 M HCl-TP methods described above.

Accretion

Accretion rates in the riparian wetlands were measured using ceramic tiles (30.5 x 30.5 cm) (McMillan and Noe 2017; Callaway et al. 2013), three per plot, placed in early October 2019. Accumulated sediment, detritus, and litter were collected from tiles and bagged during dry conditions in July of 2020. Accreted material was stored in pre-weighed and labeled zip-lock bags and then composite samples of accreted material were created. At the lab, live biomass and other contamination (plastic, tile debris) were removed, samples were dried at 60°C and weighed, and then analyzed for LOI, total P, inorganic P, and organic P, following the 3-pool parallel P fractionation method described below for soils (Richardson and Reddy 2013). The mass of sediment and detritus was then estimated as the difference between total accretion and litter.

Soil sequential soil P fractionation

Within one week following sample collection, we initiated a sequential P fractionation (SF) that separates five operational fractions of soil P (Reddy et al. 1998; Roy et al. 2017) using 1-2 g field-moist soil samples: (SF-1) readily available P [20 mL 2 M KCl extraction for 1h, analyzed for SRP], (SF-2) Fe/Al-bound Pi [20 mL 0.1 M NaOH extraction for 17-h, analyzed for SRP], (SF-3) alkali extractable Po [= 0.1 M NaOH TP – 0.1 M NaOH-Pi], (SF-4) Ca/Mg-bound Pi [20 mL 0.5 M HCl extraction for 24 hrs, analyzed for SRP] and (SF-5) residual P [nitric acid digestion on residue from SF-4, analyzed on ICP, Perkin-Elmer Avio 200 ICP-OES #0790004)] (Richardson & Reddy 2013). We calculated total P as the sum of all five fractions, organic P as the sum of fractions 3 and 5, and inorganic P as the sum of fractions 1, 2, and 4 (Figure S12).

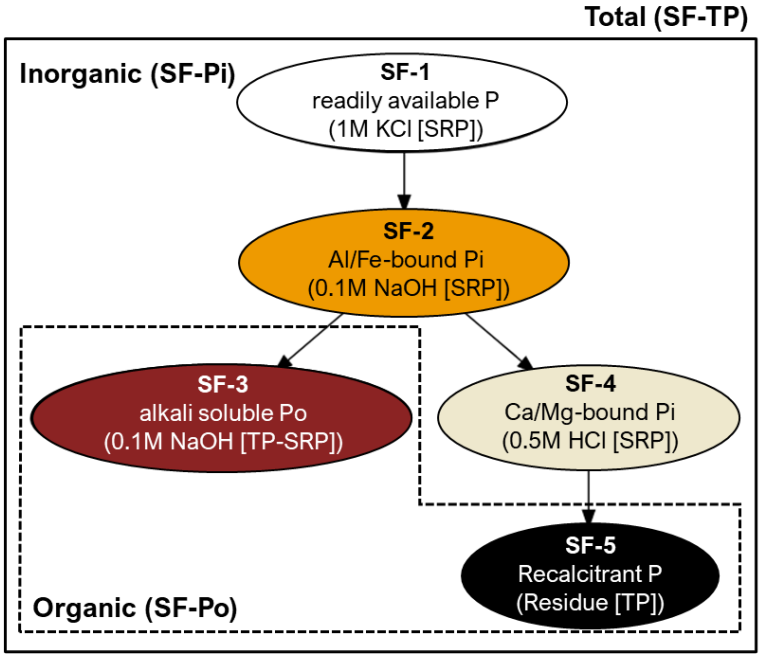

Figure S12. Flow diagram of sequential P fractionation showing inorganic and organic pools.

Soil parallel P fractionation

We also conducted a three-pool parallel fractionation (Levy & Schlesinger 1999; Richardson & Reddy 2013; Wiegman et al. 2022). For total P (HCl-TP), 0.3 g dried and ground soil subsamples

were placed into pre-weighed borosilicate glass 15 ml conical bottom extraction tubes then ashed and reweighed to estimate organic content via loss on ignition (LOI, at 550°C for 4 hrs). Ashed samples were then extracted with 15 mL (1:50 m/v) of 1M HCl for 16 hrs. For inorganic P (1 M HCl-P_i), 0.3 g dried and ground soil subsamples were placed in HDPE centrifuge tubes and extracted in the same fashion as for 1M HCl-TP. Organic P (1 M HCl-P_o) was calculated as the difference between 1M HCl-TP and 1M HCl-P_i.

Soil total elements

Total minerals, including P, Fe, Al, Ca, Mg were determined using nitric acid microwave digestion following EPA method 3051 and analysis by ICP (abbreviations: P-3051a, Fe-3051a, etc.).

Soil particle size

Particle size analysis was run on air-dried and 2mm-sieved soils after overnight dispersion in Calgon solution. Clay was determined by the hydrometer method (Bouyoucos 1962; Day 1965). Sand was determined gravimetrically by wet sieving to <53µm (sieve No. 270). Silt was calculated as the remainder. Particle sizes and texture class are from the USDA Soil Survey Manual (Soil Science Division Staff 2017).

Soil diffusion of SRP to floodwater during inundation

SRP flux is governed by sorption-desorption dynamics within the soil and the SRP concentration gradient between soil porewater and the overlying water column. Diffusive SRP flux between wetland soils and the overlying water column was estimated using an intact core method (Roy et al. 2012). Full methods and results for our study sites have been previously described in Wiegman et al. (2022).

Within one week of collection from the field, we extracted moist soils for water extractable P (WEP) [2g dry equivalent of field-moist soil in 20 mL DDI H_2O extraction for 1h, analyzed for SRP]. To better characterize P sorption dynamics within our site soils, we used batch incubations to determine phosphate sorption isotherms following Graetz & Nair (2009). Briefly air-dried and sieved soils were composited volumetrically at each plot and depth, then ~1g aliquots of soil were equilibrated for 24hrs in the dark at 4°C in 20 mL of 0.01M KCl solution with concentrations (C) of phosphate as KH_2PO_4: 0, 0.1, 0.5, 0.1, 1, 10, 75 mg P L^{-1}. The amount of sorbed P (S) is calculated from the difference in concentration before and after each incubation. The initially sorbed P (S_0) was determined as the y-intercept parameter to a linear regression fit of S and C, at values of C below 1 mg P L^{-1}. The equilibrium P concentration where net sorption and desorption equal zero (EPC_0) was determined by solving for y equals zero using the linear regression fit for S and C, at values of C below 1 mg L^{-1}. A nonlinear Langmuir model was used to determine the bond energy (K_L) and maximum P sorption (S_{max}) for the S-C relationship using all concentrations (Bolster & Hornberger 2007).

TEXT S3. ADDITIONAL RESULTS

This section includes supplemental figures and tables that provide additional detail on results. Tables S2 – S5 and figures S13 – S16 show additional results from the field study and associated statistics. Table S6 and figure S17 summarize results of *wetlandP* model scenarios described in Table 2 of the main article.

Table S2. Characteristics of flood inundation events monitored at each site. See Figure S14 for high frequency data.

Site & Event	Event driver	Peak water level (cm)	Water temperature (°C)	Dissolved oxygen (%)[c]
Prindle Rd				
October 2019	rain	20[a]	5-15	~20-80
March 2021	snowmelt	32[b]	0-12	~20-100, lowest after water level peak
April-May 2021	rain	45[b]	7-15	~0-100+
Union St				
October 2019[c]	rain	55[a]	9-15[c]	~60-90% 0d-3d, then ~50% after 3d, then ~2-25% after 10d[c]
December 2020	rain & snowmelt	85[a]	2	75% initially, 0% after 3 d, then 0-40%
March 2021	rain & snowmelt	80[a]	6-20	95% initially, 10% after 3 d, then > 50%
Swamp Rd				
October 2019	rain	45[a]	10	100% initially, 0% after 4 d, then 0-30%
December 2020	rain & snowmelt	60[a]	2	95% initially, 0% after 3.5 d, then 0-10%
March 2021	rain & snowmelt	95[a]	6-20	95% initially, 0% after 4 d, then 0-80%

Notes: [a]Water level relative to median elevation plot (plot 2). [b]Water level relative to low elevation plot (plot 0) due to movement of ISCO following drought conditions. [c]YSI data from surface water used in substitute of mini-DOT sensors due to sensor error – may not represent soil-water interface.

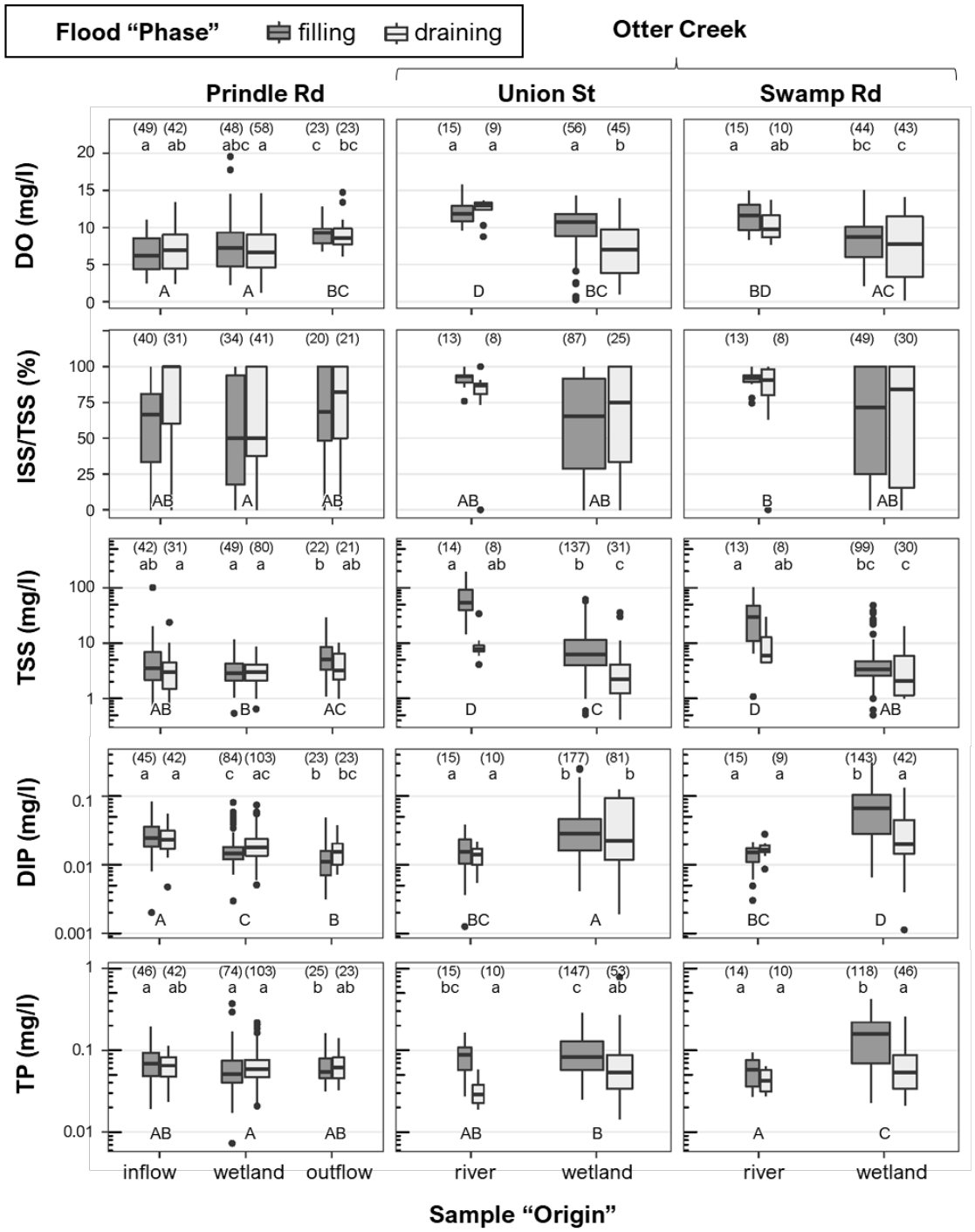

Figure S13. Box-and-whisker plots of water quality parameters in grab samples at each site. Shading of boxes denotes flood phase during sample collection - grey for filling (water level rising) and white for draining (water level falling). The number of observations is given in parentheses above each group. Letters denote significant differences among groups (origin and phase) within sites (Dunn-Bonferroni, alpha = 0.05).

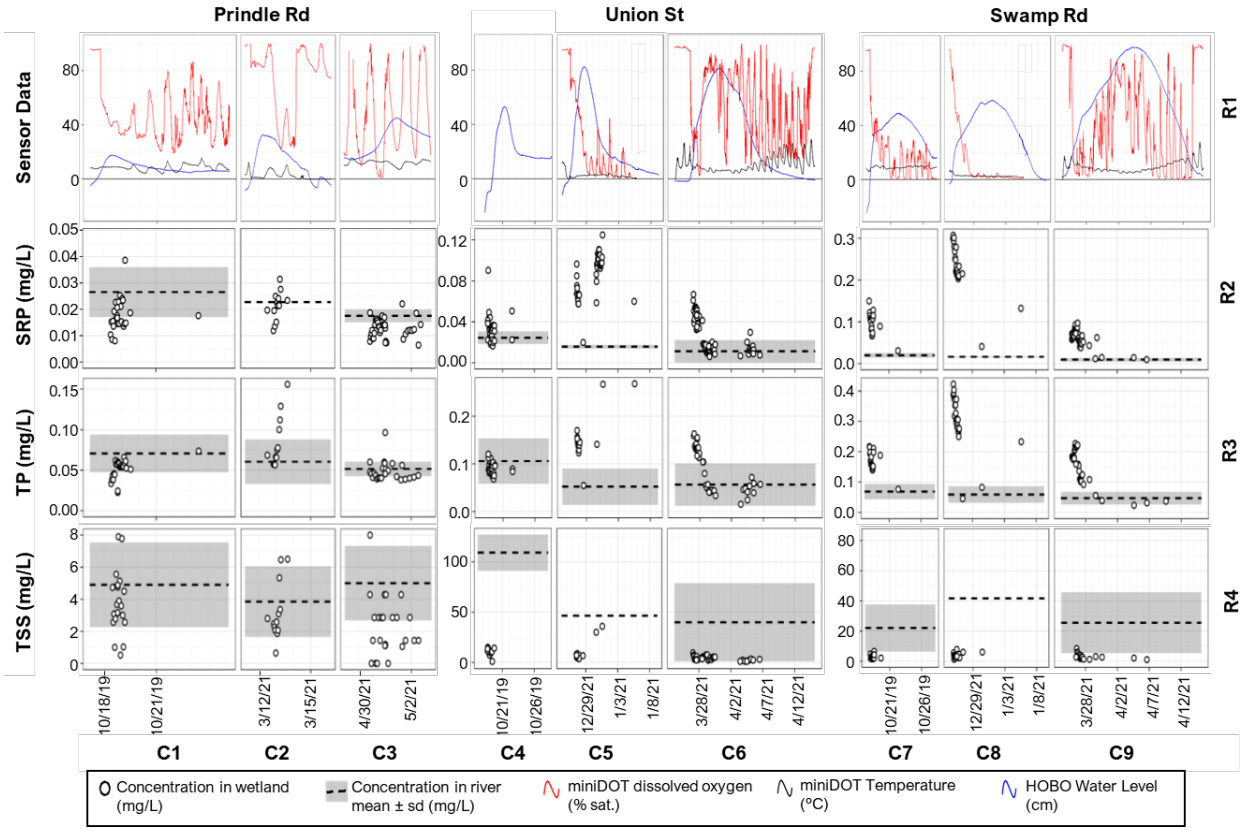

Figure S14. High frequency sensor data including water level, dissolved oxygen, and temperature (R1), and concentrations of SRP (R2), TP (R3), TSS (R4) at Prindle Rd (C1-C3), Union St (C4-C6), and Swamp Rd (C7-C9). Points show values measured in each wetland, while dashed lines and shaded area show the mean and standard deviation, respectively, of the river concentrations for each pulse. All data for Union St and Swamp Rd correspond with the median elevation plot at each site (plot 2). The data first column at Prindle Rd was collected at plot 2, while the second and third columns were collected at plot.

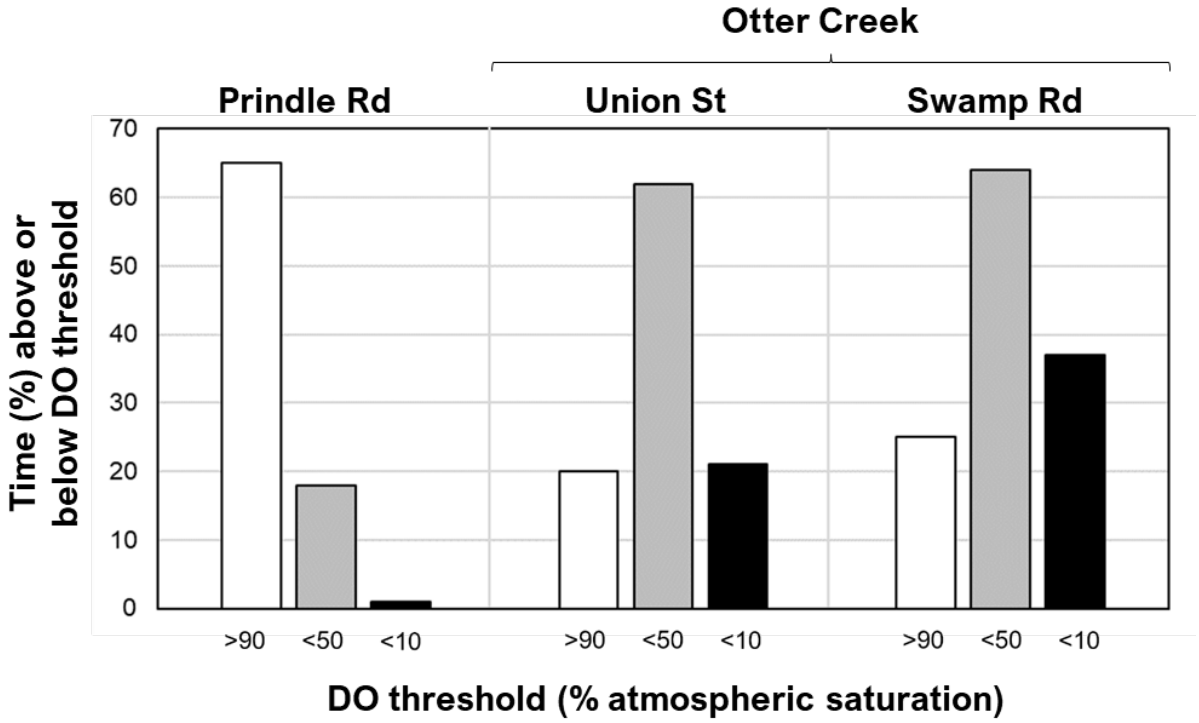

Figure S15. Percent of time that surface water dissolved oxygen (DO, % atmospheric saturation) is above/below a given threshold within the wetland during flood events. Data from PME miniDOT loggers deployed at wetland sampling plots during flood pulses at each site over the two-year monitoring period.

Table S3. Minimum, median, and maximum of plot level mean values within a given site for selected hydrology metrics, P accretion rates, and selected soil properties for 0-10cm soil layer.

	Prindle Rd			Swamp Rd			Union St		
Variable	**min**	**med**	**max**	**min**	**med**	**max**	**min**	**med**	**max**
Hydrology Metrics									
hydroperiod (d y^{-1})	139	232	361	3	192	265	15	173	321
D90% (m)	0.118	0.204	0.56	0.299	0.678	0.732	0.248	0.298	0.579
P Accretion Rates (g P m^{-2} yr^{-1})									
Total Acc. (HCl-TP)	0.286	0.368	1.15	0.398	1.38	1.68	0.224	0.715	1.25
Inorg. Acc. (HCl-Pi))	0.0866	0.121	0.292	0.127	0.763	1.03	0.0782	0.317	0.7
Org. Acc. (HCl-Po)	0.165	0.272	0.895	0.272	0.617	0.75	0.146	0.31	0.553
Litter (HCl-TP) (HCl-TP)	0.126	0.177	0.289	0.142	0.339	0.474	0.171	0.244	0.358
Total Acc. - Litter (HCl-TP)	0.153	0.195	0.877	0.208	1.06	1.21	0.0403	0.471	0.894
Soil Properties 0-10 cm									
LOI (g/g)	0.153	0.188	0.24	0.136	0.181	0.299	0.16	0.187	0.303
BD (g cm-3)	0.278	0.479	0.741	0.27	0.489	0.721	0.333	0.473	0.594
WEPw (mg P kg^{-1})	0.11	0.322	0.66	0.452	0.62	0.973	0.123	0.14	0.525
Ox-P (mmol kg^{-1})	8.69	11.5	14.1	16.2	21.7	24.6	14.9	20.2	21.3
Ox-Al (mmol kg^{-1})	75.3	79.3	126	42.3	79.4	89	64.7	69.3	84.6
Ox-Fe (mmol kg^{-1})	31.7	47.9	55.2	31.8	43.4	80.9	80.1	98.3	138
Ox-PSR(mol/mol)	0.0698	0.0832	0.121	0.132	0.166	0.225	0.0923	0.103	0.126
Ox-SPSC (mg P kg^{-1})	129	301	362	-37.4	18.5	273	286	395	497
HCl-Pi (mg P kg^{-1})	262	289	455	301	381	391	256	320	502
HCl-Po (mg P kg^{-1})	408	569	770	514	683	937	613	730	826
HCl-TP (mg P kg^{-1})	723	858	1070	904	1070	1250	935	1120	1140
SF-1 (mg P kg^{-1})	0.155	0.187	0.256	0.099	0.149	0.19	0.137	0.156	0.174
SF-2 (mg P kg^{-1})	41.3	66.7	88.4	97.7	148	153	56.1	122	219
SF-3 (mg P kg^{-1})	139	191	273	380	478	535	381	445	519
SF-4 (mg P kg^{-1})	108	189	352	171	204	259	125	200	284
SF-5 (mg P kg^{-1})	319	369	496	238	309	357	249	328	449
SF-Pi (mg P kg^{-1})	457	614	732	617	747	892	641	830	847
SF-TP (mg P kg^{-1})	676	869	1080	975	1110	1180	936	1160	1190
SF-Po (mg P kg^{-1})	183	256	441	289	352	391	182	326	467
P-3051a (mg P kg^{-1})	682	823	1050	931	1150	1260	834	1080	1140
Fe-3051a (mg Fe kg^{-1})	15400	24300	27000	20500	23500	26500	23700	28500	31300
Al-3051a (mg Al kg^{-1})	23000	30300	34300	18000	26200	28200	18700	20800	20900
Ca-3051a (mg Ca kg^{-1})	5710	6090	8380	3540	4820	5630	3590	3880	4630
Mg-3051a (mg Mg kg^{-1})	5650	7670	8090	4950	5890	6440	5050	5860	6450

Table S4. Summary of Spearman rho correlations for selected variable combinations. Only combinations where p-values < 0.05 are shown. Results are grouped by variable 1 and ordered by the absolute value of spearman rho. The HCl-TP content (mg P kg^{-1}) of aboveground herbaceous biomass, aboveground litter, and belowground biomass, are noted as AGHB-TP, AGL-TP, and BGB-TP respectively. See Table S3 for all other variable definitions and units. Of the variables in Table S1, only total P, Al, Ca, Mg, Fe for 3051a method (e.g. P-3051a) have been omitted.

Variable 1	Variable 2	Spearman rho	p-value
Inorg. Acc. (HCl-Pi)	Total Acc. (HCl-TP)	0.94	0
Inorg. Acc. (HCl-Pi)	Total Acc. (HCl-TP) - Litter (HCl-TP)	0.93	0
Inorg. Acc. (HCl-Pi)	SF-2	0.83	1.58E-04
Inorg. Acc. (HCl-Pi)	Litter (HCl-TP)	0.8	6.08E-04
Inorg. Acc. (HCl-Pi)	Org. Acc. (HCl-Po)	0.79	7.45E-04
Inorg. Acc. (HCl-Pi)	HCl-TP	0.76	0.00164
Inorg. Acc. (HCl-Pi)	AGL-TP	0.71	0.00381
Inorg. Acc. (HCl-Pi)	Ox-PSR	0.69	0.00582
Inorg. Acc. (HCl-Pi)	D90%	0.68	0.0069
Inorg. Acc. (HCl-Pi)	Ox-P	0.68	0.00729
Inorg. Acc. (HCl-Pi)	SF-TP	0.68	0.00729
Inorg. Acc. (HCl-Pi)	WEPw	0.6	0.0195
Inorg. Acc. (HCl-Pi)	HCl-Pi	0.59	0.0232
Inorg. Acc. (HCl-Pi)	SF-3	0.59	0.0232
Inorg. Acc. (HCl-Pi)	AGHB-TP	0.57	0.0298
Org. Acc. (HCl-Po)	Total Acc. (HCl-TP)	0.92	0
Org. Acc. (HCl-Po)	AGL-TP	0.91	0
Org. Acc. (HCl-Po)	Total Acc. (HCl-TP) - Litter (HCl-TP)	0.9	0
Org. Acc. (HCl-Po)	Inorg. Acc. (HCl-Pi)	0.79	7.45E-04
Org. Acc. (HCl-Po)	Litter (HCl-TP)	0.66	0.00858
Org. Acc. (HCl-Po)	hydroperiod	0.65	0.01
Org. Acc. (HCl-Po)	D90%	0.61	0.0187
Org. Acc. (HCl-Po)	HCl-Pi	0.57	0.0298
Org. Acc. (HCl-Po)	SF-2	0.57	0.0275
Org. Acc. (HCl-Po)	WEPw	0.54	0.0407
Total Acc. (HCl-TP)	Total Acc. (HCl-TP) - Litter (HCl-TP)	0.99	0
Total Acc. (HCl-TP)	Inorg. Acc. (HCl-Pi)	0.94	0
Total Acc. (HCl-TP)	Org. Acc. (HCl-Po)	0.92	0
Total Acc. (HCl-TP)	AGL-TP	0.86	8.57E-06
Total Acc. (HCl-TP)	Litter (HCl-TP)	0.79	6.74E-04
Total Acc. (HCl-TP)	D90%	0.74	0.00221
Total Acc. (HCl-TP)	SF-2	0.72	0.00313
Total Acc. (HCl-TP)	Ox-PSR	0.61	0.0187
Total Acc. (HCl-TP)	WEPw	0.6	0.0204
Total Acc. (HCl-TP)	HCl-TP	0.6	0.0213
Total Acc. (HCl-TP)	HCl-Pi	0.59	0.0243
Total Acc. (HCl-TP)	hydroperiod	0.53	0.0454
Total Acc. (HCl-TP) - Litter (HCl-TP)	Total Acc. (HCl-TP)	0.99	0

Variable 1	Variable 2	Spearman rho	p-value
Total Acc. (HCl-TP) - Litter (HCl-TP)	Inorg. Acc. (HCl-Pi)	0.93	0
Total Acc. (HCl-TP) - Litter (HCl-TP)	Org. Acc. (HCl-Po)	0.9	0
Total Acc. (HCl-TP) - Litter (HCl-TP)	AGL-TP	0.81	3.40E-04
Total Acc. (HCl-TP) - Litter (HCl-TP)	D90%	0.76	0.00139
Total Acc. (HCl-TP) - Litter (HCl-TP)	Litter (HCl-TP)	0.7	0.00459
Total Acc. (HCl-TP) - Litter (HCl-TP)	SF-2	0.69	0.00549
Total Acc. (HCl-TP) - Litter (HCl-TP)	HCl-TP	0.62	0.0149
Total Acc. (HCl-TP) - Litter (HCl-TP)	HCl-Pi	0.59	0.0223
Total Acc. (HCl-TP) - Litter (HCl-TP)	Ox-PSR	0.57	0.0298
Total Acc. (HCl-TP) - Litter (HCl-TP)	WEPw	0.56	0.031
Total Acc. (HCl-TP) - Litter (HCl-TP)	hydroperiod	0.54	0.0407
AGHB-TP	Ox-PSR	0.79	7.45E-04
AGHB-TP	SF-3	0.74	0.00255
AGHB-TP	D90%	0.65	0.0111
AGHB-TP	SF-TP	0.65	0.0111
AGHB-TP	Ox-P	0.62	0.0149
AGHB-TP	HCl-TP	0.62	0.0149
AGHB-TP	SF-Po	0.58	0.0253
AGHB-TP	Inorg. Acc. (HCl-Pi)	0.57	0.0298
AGL-TP	Org. Acc. (HCl-Po)	0.91	0
AGL-TP	Total Acc. (HCl-TP)	0.86	8.57E-06
AGL-TP	Total Acc. (HCl-TP) - Litter (HCl-TP)	0.81	3.40E-04
AGL-TP	Litter (HCl-TP)	0.72	0.00357
AGL-TP	Inorg. Acc. (HCl-Pi)	0.71	0.00381
AGL-TP	D90%	0.68	0.00729
AGL-TP	WEPw	0.61	0.0171
AGL-TP	hydroperiod	0.58	0.0264
AGL-TP	HCl-Pi	0.58	0.0253
AGL-TP	Ox-SPSC	-0.55	0.0349
AGL-TP	SF-2	0.53	0.0454
BGB-TP	SF-1	-0.67	0.0077
BGB-TP	SF-Po	0.57	0.0286
BGB-TP	HCl-TP	0.53	0.0438
D90%	Total Acc. (HCl-TP) - Litter (HCl-TP)	0.76	0.00139
D90%	Total Acc. (HCl-TP)	0.74	0.00221
D90%	Ox-PSR	0.73	0.00273
D90%	WEPw	0.7	0.00518
D90%	Inorg. Acc. (HCl-Pi)	0.68	0.0069
D90%	AGL-TP	0.68	0.00729
D90%	AGHB-TP	0.65	0.0111
D90%	Org. Acc. (HCl-Po)	0.61	0.0187
D90%	Ox-SPSC	-0.58	0.0264
D90%	Litter (HCl-TP)	0.57	0.0298
D90%	HCl-Pi	0.52	0.0488
HCl-Pi	SF-Pi	0.81	4.35E-04

Variable 1	Variable 2	Spearman rho	p-value
HCl-Pi	SF-2	0.78	9.88E-04
HCl-Pi	Total Acc. (HCl-TP)	0.59	0.0243
HCl-Pi	Inorg. Acc. (HCl-Pi)	0.59	0.0232
HCl-Pi	Total Acc. (HCl-TP) - Litter (HCl-TP)	0.59	0.0223
HCl-Pi	AGL-TP	0.58	0.0253
HCl-Pi	Ox-PSR	0.58	0.0264
HCl-Pi	Org. Acc. (HCl-Po)	0.57	0.0298
HCl-Pi	WEPw	0.53	0.0454
HCl-Pi	D90%	0.52	0.0488
HCl-Po	SF-Po	0.95	0
HCl-Po	HCl-TP	0.87	0
HCl-Po	SF-TP	0.85	4.10E-05
HCl-Po	SF-3	0.78	9.88E-04
HCl-Po	Ox-P	0.57	0.0275
HCl-Po	SF-1	-0.54	0.0407
HCl-TP	SF-TP	0.96	0
HCl-TP	HCl-Po	0.87	0
HCl-TP	SF-Po	0.87	0
HCl-TP	SF-3	0.82	2.97E-04
HCl-TP	Inorg. Acc. (HCl-Pi)	0.76	0.00164
HCl-TP	Ox-P	0.73	0.00273
HCl-TP	AGHB-TP	0.62	0.0149
HCl-TP	Total Acc. (HCl-TP) - Litter (HCl-TP)	0.62	0.0149
HCl-TP	Total Acc. (HCl-TP)	0.6	0.0213
HCl-TP	Ox-PSR	0.58	0.0253
HCl-TP	SF-2	0.58	0.0264
HCl-TP	BGB-TP	0.53	0.0438
hydroperiod	LOI	0.66	0.00953
hydroperiod	Org. Acc. (HCl-Po)	0.65	0.01
hydroperiod	AGL-TP	0.58	0.0264
hydroperiod	Ox-Al	0.56	0.0336
hydroperiod	Total Acc. (HCl-TP) - Litter (HCl-TP)	0.54	0.0407
hydroperiod	Total Acc. (HCl-TP)	0.53	0.0454
LOI	hydroperiod	0.66	0.00953
LOI	Ox-Al	0.54	0.0407
Ox-Al	hydroperiod	0.56	0.0336
Ox-Al	LOI	0.54	0.0407
Ox-Fe	Ox-SPSC	0.79	8.21E-04
Ox-Fe	WEPw	-0.59	0.0243
Ox-P	SF-2	0.81	3.40E-04
Ox-P	SF-TP	0.77	0.00128
Ox-P	Ox-PSR	0.76	0.00139
Ox-P	SF-3	0.74	0.00255
Ox-P	HCl-TP	0.73	0.00273
Ox-P	Inorg. Acc. (HCl-Pi)	0.68	0.00729

Variable 1	Variable 2	Spearman rho	p-value
Ox-P	AGHB-TP	0.62	0.0149
Ox-P	SF-Po	0.59	0.0232
Ox-P	HCl-Po	0.57	0.0275
Ox-P	Litter (HCl-TP)	0.55	0.0349
Ox-P	SF-Pi	0.55	0.0363
Ox-PSR	AGHB-TP	0.79	7.45E-04
Ox-PSR	WEPw	0.78	9.02E-04
Ox-PSR	Ox-P	0.76	0.00139
Ox-PSR	Ox-SPSC	-0.73	0.00273
Ox-PSR	D90%	0.73	0.00273
Ox-PSR	SF-2	0.72	0.00334
Ox-PSR	SF-3	0.7	0.00488
Ox-PSR	Inorg. Acc. (HCl-Pi)	0.69	0.00582
Ox-PSR	SF-Pi	0.64	0.0123
Ox-PSR	Litter (HCl-TP)	0.62	0.0149
Ox-PSR	Total Acc. (HCl-TP)	0.61	0.0187
Ox-PSR	SF-TP	0.61	0.0187
Ox-PSR	HCl-Pi	0.58	0.0264
Ox-PSR	HCl-TP	0.58	0.0253
Ox-PSR	Total Acc. (HCl-TP) - Litter (HCl-TP)	0.57	0.0298
Ox-PSR	SF-5	-0.52	0.0471
Ox-SPSC	WEPw	-0.85	2.39E-05
Ox-SPSC	Ox-Fe	0.79	8.21E-04
Ox-SPSC	Ox-PSR	-0.73	0.00273
Ox-SPSC	D90%	-0.58	0.0264
Ox-SPSC	AGL-TP	-0.55	0.0349
SF-Po	HCl-Po	0.95	0
SF-Po	HCl-TP	0.87	0
SF-Po	SF-3	0.86	0
SF-Po	SF-TP	0.85	4.10E-05
SF-Po	Ox-P	0.59	0.0232
SF-Po	AGHB-TP	0.58	0.0253
SF-Po	BGB-TP	0.57	0.0286
SF-Po	SF-1	-0.56	0.0336
SF-Pi	SF-4	0.83	1.88E-04
SF-Pi	HCl-Pi	0.81	4.35E-04
SF-Pi	Ox-PSR	0.64	0.0123
SF-Pi	SF-2	0.62	0.0149
SF-Pi	Ox-P	0.55	0.0363
SF-Pi	WEPw	0.54	0.0392
SF-TP	HCl-TP	0.96	0
SF-TP	HCl-Po	0.85	4.10E-05
SF-TP	SF-Po	0.85	4.10E-05
SF-TP	SF-3	0.83	1.58E-04
SF-TP	Ox-P	0.77	0.00128

Variable 1	Variable 2	Spearman rho	p-value
SF-TP	Inorg. Acc. (HCl-Pi)	0.68	0.00729
SF-TP	AGHB-TP	0.65	0.0111
SF-TP	Ox-PSR	0.61	0.0187
SF-TP	SF-2	0.57	0.0298
SF-1	BGB-TP	-0.67	0.0077
SF-1	SF-Po	-0.56	0.0336
SF-1	HCl-Po	-0.54	0.0407
SF-2	Inorg. Acc. (HCl-Pi)	0.83	1.58E-04
SF-2	Ox-P	0.81	3.40E-04
SF-2	HCl-Pi	0.78	9.88E-04
SF-2	Litter (HCl-TP)	0.75	0.00205
SF-2	Total Acc. (HCl-TP)	0.72	0.00313
SF-2	Ox-PSR	0.72	0.00334
SF-2	Total Acc. (HCl-TP) - Litter (HCl-TP)	0.69	0.00549
SF-2	SF-Pi	0.62	0.0149
SF-2	HCl-TP	0.58	0.0264
SF-2	Org. Acc. (HCl-Po)	0.57	0.0275
SF-2	SF-TP	0.57	0.0298
SF-2	AGL-TP	0.53	0.0454
SF-2	WEPw	0.53	0.0454
SF-3	SF-Po	0.86	0
SF-3	SF-TP	0.83	1.58E-04
SF-3	HCl-TP	0.82	2.97E-04
SF-3	HCl-Po	0.78	9.88E-04
SF-3	AGHB-TP	0.74	0.00255
SF-3	Ox-P	0.74	0.00255
SF-3	Ox-PSR	0.7	0.00488
SF-3	Inorg. Acc. (HCl-Pi)	0.59	0.0232
SF-4	SF-Pi	0.83	1.88E-04
SF-5	Ox-PSR	-0.52	0.0471
WEPw	Ox-SPSC	-0.85	2.39E-05
WEPw	Ox-PSR	0.78	9.02E-04
WEPw	D90%	0.7	0.00518
WEPw	AGL-TP	0.61	0.0171
WEPw	Total Acc. (HCl-TP)	0.6	0.0204
WEPw	Inorg. Acc. (HCl-Pi)	0.6	0.0195
WEPw	Ox-Fe	-0.59	0.0243
WEPw	Total Acc. (HCl-TP) - Litter (HCl-TP)	0.56	0.031
WEPw	Org. Acc. (HCl-Po)	0.54	0.0407
WEPw	Litter (HCl-TP)	0.54	0.0422
WEPw	SF-Pi	0.54	0.0392
WEPw	HCl-Pi	0.53	0.0454
WEPw	SF-2	0.53	0.0454

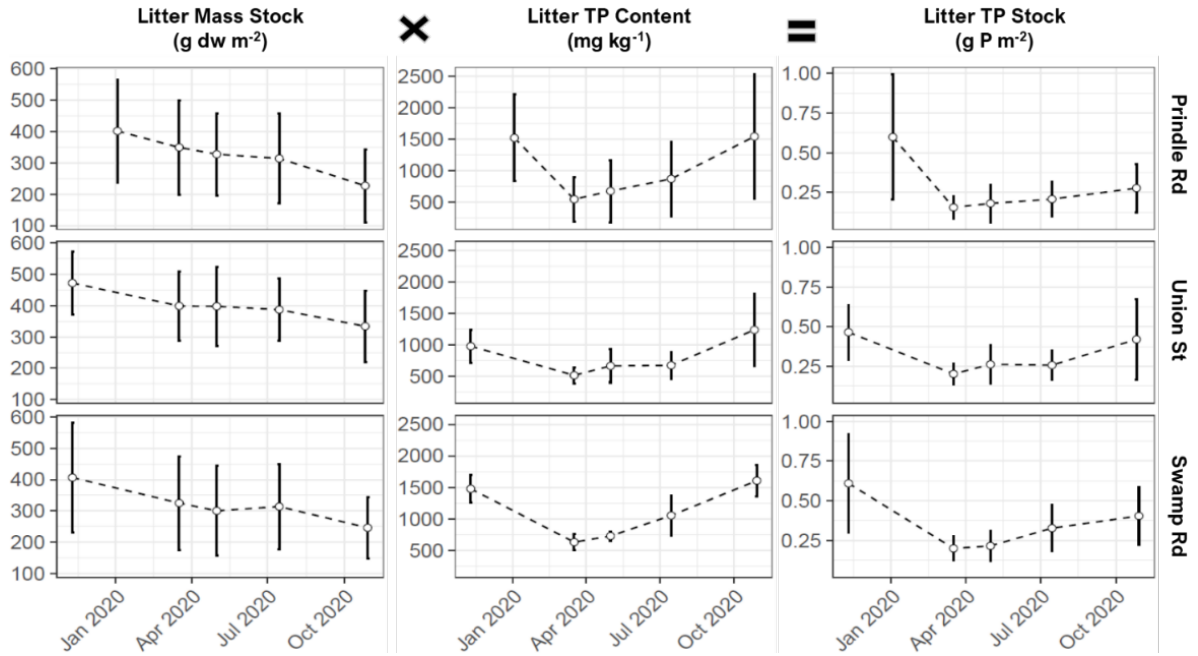

Figure S16. A matrix of litterbag decomposition results for each study site (rows), points denote site level means for each site, vertical bars denote standard deviation.

Table S5. Soil to water SRP flux rates observed in simulated floods inside intact cores (average flux rate over the first 7 days after flooding) and related soil properties (reported as averages for the top 0-5cm).

site	**Prindle Road**			**Union Street**			**Swamp Road**		
plot	**0**	**2**	**4**	**0**	**2**	**4**	**0**	**2**	**4**
Intact Core SRP flux rates (g P m^{-2} d^{-1}) - Day 0 to 7									
Anaerobic	0.024 ± 0.017	0.019 ± 0.008	0.017 ± 0.003	0.009 ± 0.005	0.004 ± 0.001	0.005 ± 0.002	0.029 ± 0.015	0.031 ± 0.024	0.01 ± 0.005
Aerobic	0.004 ± 0.002	0.008 ± 0.006	0.015 ± 0.016	0.003 ± 0.001	0.002 ± 0.001	0.003 ± 0.001	0.006 ± 0.003	0.007 ± 0.004	0.004 ± 0.001
Soil Properties - Depth 0 to 5cm									
WEP (mg/kg)	0.47 ± 0.25	0.13 ± 0.13	0.18 ± 0.27	0.57 ± 0.29	0.07 ± 0.11	0.06 ± 0.09	2.45 ± 2.35	0.27 ± 0.41	0.44 ± 0.22
Ox-[P:Fe] (mol/mol)	0.35 ± 0.02	0.3 ± 0.04	0.27 ± 0.01	0.25 ± 0.05	0.22 ± 0.03	0.16 ± 0.03	0.37 ± 0.1	0.53 ± 0.1	0.23 ± 0.01
Ox-[P:Al] (mol/mol)	0.18 ± 0.2	0.17 ± 0.25	0.15 ± 0.14	0.26 ± 1.28	0.29 ± 0.25	0.23 ± 0.95	0.24 ± 0.22	0.31 ± 0.25	0.37 ± 0.22
Ox- PSR (mol/mol)	0.12 ± 0	0.11 ± 0.01	0.1 ± 0	0.13 ± 0.02	0.12 ± 0.01	0.09 ± 0.02	0.14 ± 0.02	0.2 ± 0.01	0.14 ± 0.01
Ox-SPSC (mg/kg)	339 ± 35	457 ± 40	484 ± 82	539 ± 155	543 ± 113	672 ± 97	324 ± 61	127 ± 60	311 ± 55
S_{max} (mg/kg)	635 ± 23	558 ± 25	438 ± 8	652 ± 7	653 ± 5	586 ± 30	925 ± 9	644 ± 23	405 ± 21
K_L (L/mg)	0.035 ± 0.003	0.063 ± 0.009	0.082 ± 0.005	0.328 ± 0.015	0.282 ± 0.009	0.056 ± 0.009	0.054 ± 0.001	0.144 ± 0.02	0.101 ± 0.019
EPC_0 (mg/L)	2.47	0.46	0.2	0.05	0.06	0.27	1.16	0.23	0.09

Table S6. Summary statistics for selected combinations of *wetlandP* simulations of study plots 0, 2, 4 for Prindle Rd, Swamp Rd, and Union St. See Table 2 in main article for description of scenarios.

P pool:	**TP**		**DIP**	
Metric:	**balance**	**efficiency**	**balance**	**efficiency**
Calculation:	**in - out**	**100*(in - out)/in**	**in - out**	**100*(in - out)/in**
Units:	**(g P m^{-2} yr^{-1})**	**%**	**(g P m^{-2} yr^{-1})**	**%**
(A) all scenarios described in table 2 of main article (n=271[a])				
mean	0.13	29.12	-0.02	-23.96
sd[b]	0.28	27.45	0.05	61.32
min	-0.06	-54.39	-0.13	-258.30
max	2.38	95.43	0.14	91.32
mean ± sd	0.13 ± 0.28	29 ± 27	-0.02 ± 0.05	-24 ± 61
% neg.[c]		8%		71%
(B) [‡]**plausible range of conditions:** power HRT only, stream concentrations only (0.5x, 1x, and 2x), observed water levels (1x and 1.2x), 100% trapping and Stokes' Law (n=108[a])				
mean	0.09	35	-0.03	-43
sd[b]	0.10	30	0.04	69
min	-0.06	-54	-0.11	-261
max	0.45	78	0.02	31
mean ± sd	0.09 ± 0.1	35 ± 30	-0.03 ± 0.04	-43 ± 69
% neg. [c]		12%		75%
(C) Same as B except 100% trapping only for particle settling (n=54[a])				
mean	0.12	51	-0.03	-43
sd[b]	0.12	26	0.04	70
min	-0.02	-21	-0.11	-261
max	0.45	78	0.02	31
mean ± sd	0.12 ± 0.12	51 ± 26	-0.03 ± 0.04	-43 ± 70
% neg. [c]		9%		76%
(D) same as B except Stokes' Law only for particle settling (n=54[a])				
mean	0.055	20	-0.028	-42
sd[b]	0.068	25	0.041	69
min	-0.062	-54	-0.113	-258
max	0.268	46	0.017	31
mean ± sd	0.05 ± 0.07	20 ± 25	-0.03 ± 0.04	-42 ± 69
% neg. [c]		15%		74%
(E) stream concentrations (1x only), water levels (1x and 1.2x), power model HRT (n=28[a])				
mean	0.07	39	-0.03	-34
sd[b]	0.05	24	0.04	46
min	-0.01	-10	-0.11	-123
max	0.21	76	0.01	27
mean ± sd	0.07 ± 0.05	39 ± 24	-0.03 ± 0.04	-34 ± 46
% neg. [c]		4%		67%

Notes: [a]number of simulations, [b]standard deviation, [c]percent of simulations where P balance and efficiency are negative, [‡] this combination represents the "plausible range of conditions" reported in the main article.

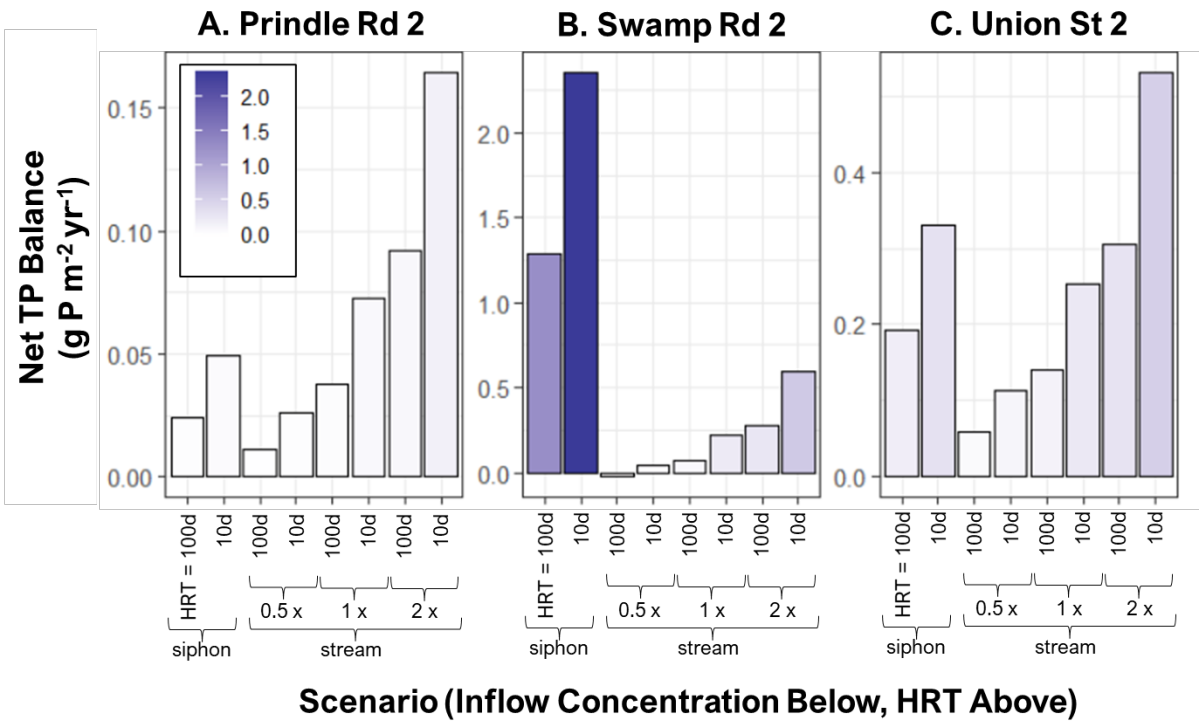

Figure S17. Comparison of concentration verses HRT driven changes on net TP balance assuming 100% particle trapping. Concentrations include siphon data, and stream medians multiplied by a factor of 0.5, 1 and 2, while HRT is varied between 10 and 100 days. The color scale is for net TP balance and applies to panels A, B, and C.

TEXT S4. FLOW ANALYSIS

This supplementary text presents a summary of flow analyses for regional USGS streamflow gauges that are relied upon to contextualize observed flood pulse events recorded at our study sites, as well as results of modeled scenarios.

Closest streamflow gauges to the study sites are:

- Prindle Brook: Lewis Creek at North Ferrisburg VT (Station #04282780) – downstream
- Union Street: Otter Creek at Center Rutland VT (Station #04282000) – upstream
- Swamp Road: Otter Creek at Middlebury VT (Station #04282500) – downstream

Analyses included: (1) a flow frequency analysis of the available long-term record for each station; (2) construction of annualized and seasonal flow duration curves; and (3) trend analysis on the frequency of exceedance for select flow thresholds. Findings are summarized here and then in more detail in the following sections.

Hydrologic conditions during the study period were near normal and did not include extremes in discharge. Each of the flood pulses we captured at Prindle Rd corresponded to a discharge event on the Lewis Creek lower in magnitude than an Annual Exceedance Probability (AEP) of 50% or a 2-year Recurrence Interval (RI). Two of the monitored inundation events at the Otter Creek sites corresponded to peak discharge values at the nearby USGS gages lower in magnitude than an AEP of 50% (2-year RI). The December 2020 event corresponded to an approximate AEP 50% event at the Otter Creek Center Rutland gage. Therefore, our results are most relevant for regular flood inundation events occurring in these wetlands on approximately 1- to 2-year recurrence intervals.

Flow frequency analysis

Peak discharges for a range of design storms were estimated for study area gauges using two methods: Log-Pearson Type III analysis and by reference to regional regression equations.

Log-Pearson Type III analysis (HEC-SSP) method

Peak discharge at a range of recurrence intervals was determined by examination of the available record of annual instantaneous peak discharges using a log-Pearson Type III analysis following Bulletin 17C procedures (England et al. 2015). This method uses the Expected Moments Algorithm to estimate the moments and parameters of the log-Pearson Type III distribution. A weighted skew approach considered the Vermont regional skew coefficient (0.44) and mean square error (0.078) developed by Olson (2014) to mitigate the sensitivity to outliers of site skew coefficients (Interagency Advisory Committee on Water Data 1982). Low outliers were detected and identified using the Multiple Grubbs-Beck method (Cohn et al. 2013). Plotting positions were calculated by the Hirsch-Stedinger method (Hirsch and Stedinger 1987). Peak annual discharge data were retrieved from the National Water Information System from the approved records (USGS, 2021). Flow frequency analysis was performed using Hydrologic Engineering Center's Statistical Software Package (HEC-SSP, v.2.2) software (USACE 2019).

Regional regression equations (Streamstats) method

Peak discharge was also estimated from a multiple linear regression model of Olsen (2014) that underlies USGS Streamstats (https://streamstats.usgs.gov/ss/) in the Vermont region. This source uses a set of equations for various return intervals to estimate peak discharge for ungauged sites on rivers minimally affected by flow regulation (e.g., withdrawals, impoundments, diversions). Generalized least-squares regression relationships were derived between peak discharge and catchment attributes for 153 streamflow gauges in and around Vermont. Peak discharges for these 153 gauges were estimated using Log-Pearson Type III analysis updated for treatment of historical and censored peak discharges – using the Expected Moments Algorithm of Cohn and others (1997, 2001). Final regression equations reflect a relationship between peak discharge and the following three independent variables: drainage area, percent wetlands/water, and mean annual precipitation.

Summary of flow frequency analysis

Peak discharges for a variety of recurrence intervals are summarized for each streamflow station in Table S7. Reasonable agreement is evident between HEC-SSP and Streamstats estimates for the Lewis Creek gauge and for the Otter Creek at Center Rutland gauge. Some degree of difference is expected because the underlying predictive equations for Streamstats are generalized regression equations based on 153 state-wide gauges with a range of attributes (Olson 2014). However, Streamstats is a poor predictor of peak discharges at the Otter Creek Middlebury gauge, largely due to attenuation of flood waves by extensive wetland complexes located between the Rutland and Middlebury gauges (Watson et al. 2016).

Flow duration curves

Flow duration curves were initially built on the most recent 29 years of daily mean discharge values for each streamflow gauge (to be consistent with the available record for Lewis Creek). Discharge data were downloaded from USGS, aggregated to water years (Oct 1 through Sept 30), and values for leap years were omitted. To enable a historic review of flow duration curves for the Otter Creek sites, which had a longer record length, two additional time periods were analyzed (1961-1989 and 1931-1959). These record lengths were also 29 years in duration to ensure balanced data sets when comparing to the most recent 29-year record. To enable comparison between study sites, flow duration values were normalized by drainage area. Flow duration curves were coded in the R programming language.

To facilitate a review of seasonal patterns, daily mean flow data were further stratified by seasons, defined as Winter (Dec-Jan-Feb), Spring (Mar-Apr-May) and the Summer/Fall growing season (Jun-Jul-Aug-Sep-Oct-Nov).

Summary of flow duration curves for study area gauges

The annual flow duration curve for each study area gauge based on the most recent 29-year record (water years 1991-2019) is presented in Figure S18. When normalized to drainage area, low-frequency discharges (>Qp90) at the Middlebury station (drainage area = 631 mi^2) are lower in magnitude that the Center Rutland station (308 mi^2). This phenomenon reflects attenuation of floodwaters by the well-connected wetland complexes between Rutland and Middlebury. A slightly steeper flow duration curve is evident for Lewis Creek (Figure S19).

Table S7. Summary of flow frequency estimates for study area streamflow gauges

					Peak Discharge (cfs)					
Station Description	Station No.	Drainage Area (sq mi)	Record Length	*Annual Exceedance Probability (%)*	50	20	10	4	2	1
				Recurrence Interval (yrs)	2	5	10	25	50	100
Otter Creek at Center Rutland	04282000	308	1929-2019	HEC-SSP	5,187	7,366	8,907	10,130	12,575	14,253
			-	*Streamstats*	*7,700*	*11,600*	*14,500*	*18,600*	*22,100*	*25,700*
Otter Creek at Middlebury	04282500	631	1928-2020	HEC-SSP	4,168	5,652	6,723	7,300	9,338	10,566
			-	*Streamstats*	*11,500*	*16,800*	*20,700*	*26,300*	*30,900*	*35,500*
Lewis Creek at North Ferrisburg	04282780	76.6	1990-2019	HEC-SSP	1,898	2,928	3,724	4,500	5,821	6,866
			-	*Streamstats*	*1,500*	*2,260*	*2,820*	*3,620*	*4,300*	*5,000*

Notes:

1. Beginning date of record for Middlebury station was truncated at 1928, due to gaps in the prior record.
2. As of March 2021, the approved records for the Middlebury station extended through 2020; for the Rutland station extended through 2019.

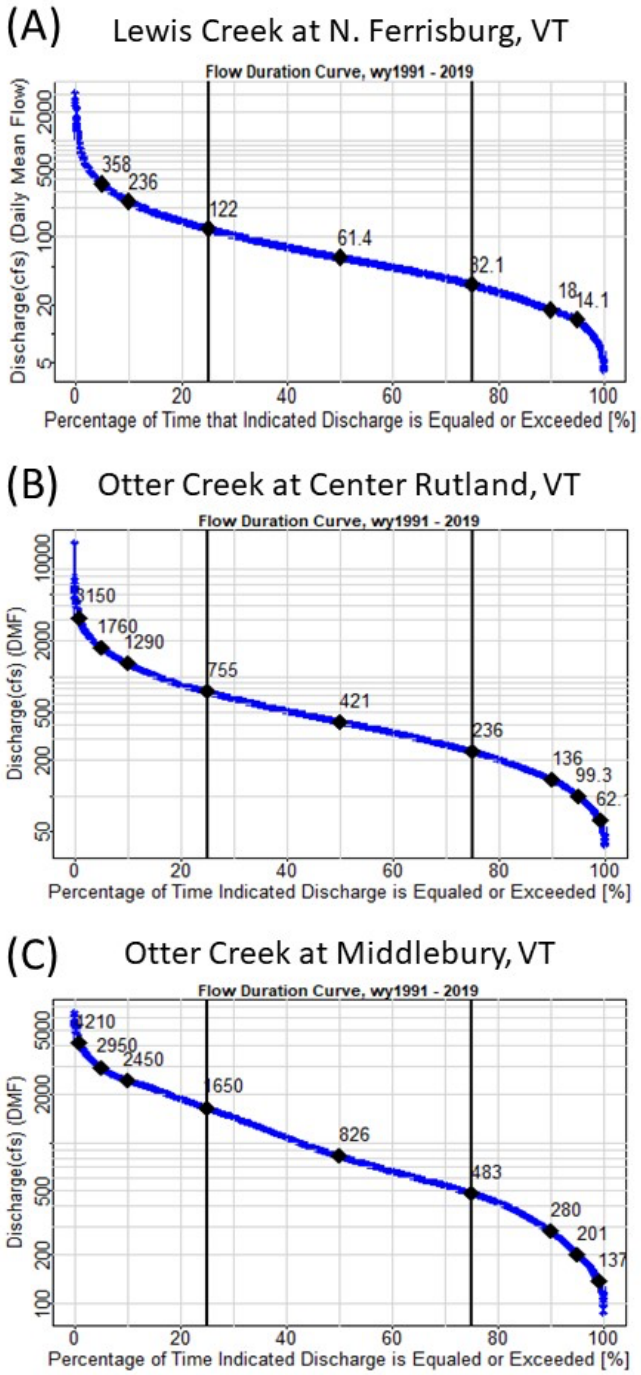

Figure S18. Flow duration curves built on daily mean discharge recorded between water years 1991 and 2019 for (A) Lewis Creek at N. Ferrisburg VT, (B) Otter Creek at Middlebury VT and (C) Otter Creek at Center Rutland, VT.

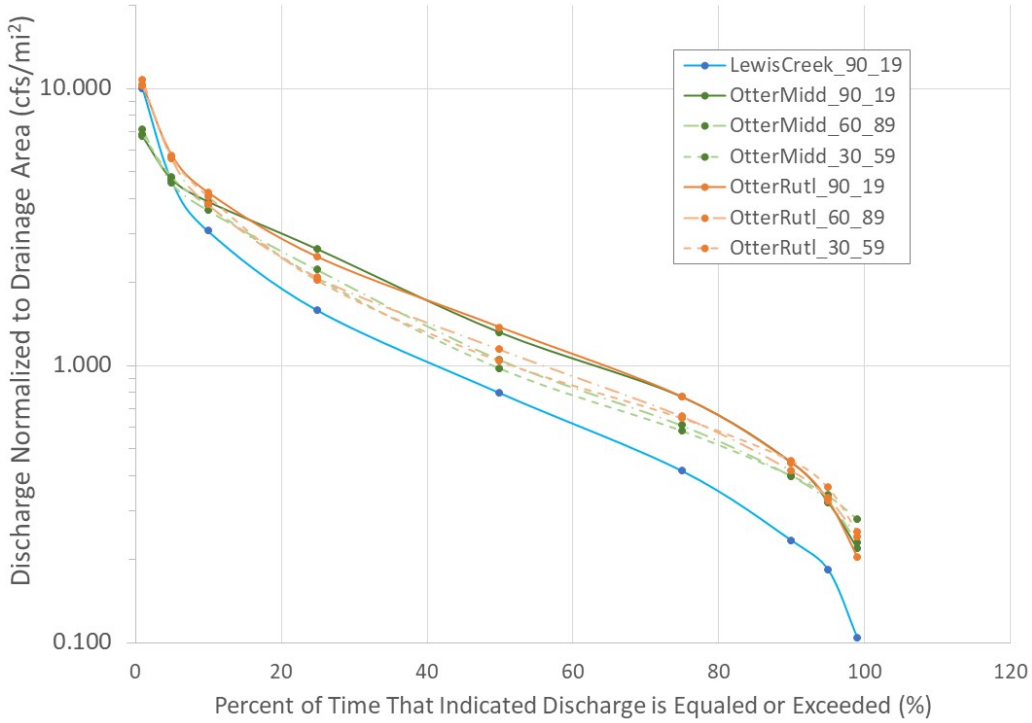

Figure S19. Annual flow duration curves developed on daily mean flow records for the Middlebury (green) and Center Rutland (orange) USGS streamflow gages on the Otter Creek alongside Lewis Creek (teal). Otter Creek records are stratified by the most recent 29 water years (to be consistent with the available record for Lewis Creek), and previous 29-year records from water years 1961-1989 and 1931-1959. Discharge values are normalized by drainage area so that records for the three stations can be more directly compared.

Retrospective analysis of flow duration curves for Otter Creek stations

The longer available discharge record for the Center Rutland and Middlebury gauges on Otter Creek allowed for a retrospective and analysis of flow duration curves on an annual and seasonal basis. When the most recent 29-year record was compared to the records for water years 1961-1989 and 1931-1959, a shift in the flow duration curve was evident in the range of Qp25 to Qp75 (Figure S19). In other words, discharges in these middle percentiles have increased in the recent 29 years as compared to previous decades. However, on an annualized basis, no substantial shift was evident in discharges greater than or equal to Qp90, at magnitudes that would be associated with overbank flooding at the Union Street and Swamp Road sites (see next section).

In the range of flows typically associated with floodplain overtopping (> Qp90), there was some evidence of shifting magnitudes over recent decades, when the Otter Creek flow duration curves were stratified by season. A somewhat higher magnitude of these low-frequency events occurred in winter months (Dec-Jan-Feb) in the most recent 29 years as compared to previous decades (Figure S20), possibly due to more precipitation falling as rain instead of snow, more rain-on-snow events, and earlier thaw events associated with rising winter temperatures (Betts 2011). Earlier timing of snow-melt related streamflows has been documented for northeast rivers (Hodgkins and Dudley 2006; Dudley et al. 2017).

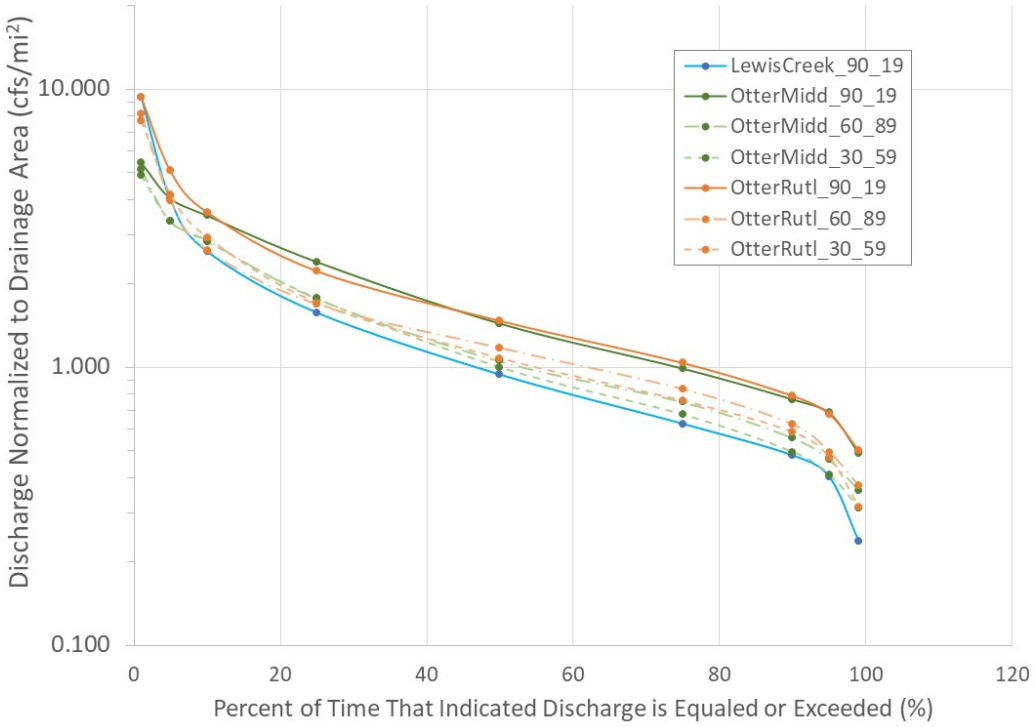

Figure S20. Winter seasonal (Dec-Jan-Feb) flow duration curves

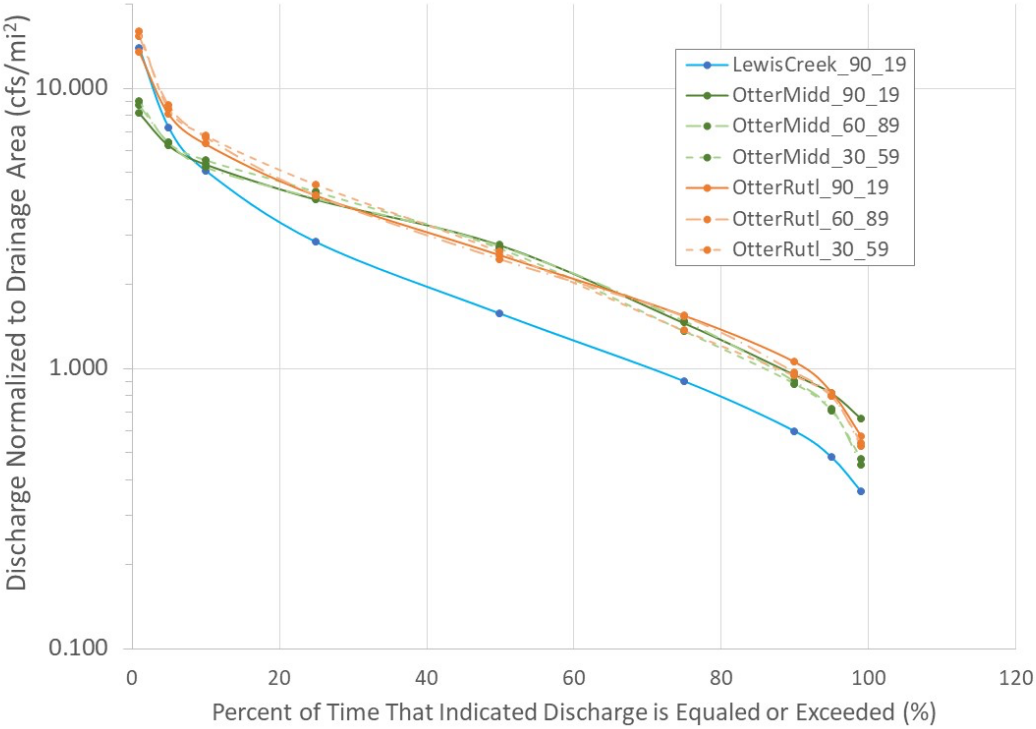

Figure S21. Spring seasonal (Mar-Apr-May) flow duration curves

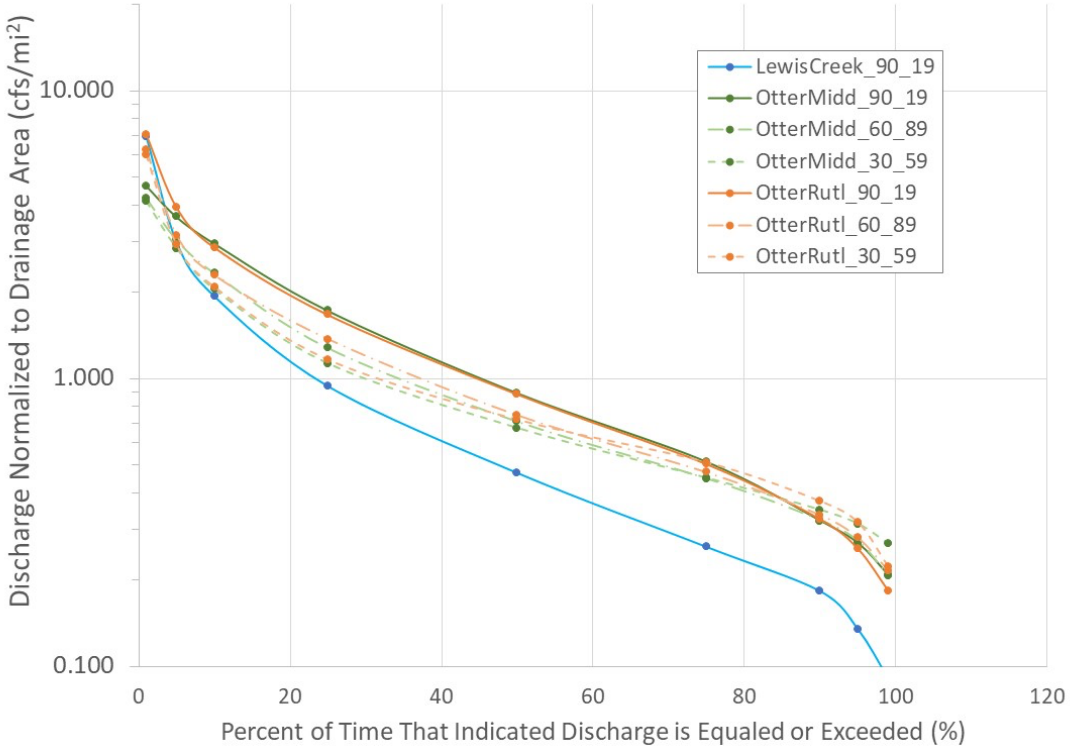

Figure S22. Summer/Fall growing season (Jun-Jul-Aug-Sep-Oct-Nov) flow duration curves

A somewhat higher magnitude of low-frequency events is also evident in the Summer/Fall growing season in the most recent 29 years as compared to previous decades (Figure S22), but in general the magnitude of these extreme events is lesser than in other seasons. Mid-range flows (>Qp50) are also elevated in the recent 29 years. This finding is consistent with regional studies that have documented increasing summer base flows, driven by increased summer precipitation magnitude (Hodgkins & Dudley, 2011). These patterns may also reflect a increasing persistence of rainfall (wet days following wet days) in the Northeast documented by Guilbert and others (2015).

Characterization of flood pulse events recorded at study sites

Relying on the above flow frequency analysis and flow duration curves, as well as sensor data, we characterized the relative magnitude of flood pulse events sampled at each site.

Lewis Creek – Prindle Brook

Flood pulses at the Prindle Brook site represented inundation events within an instream wetland that is transiently-impounded above a beaver dam. Three flood pulse events were sampled at this site for water quality parameters (Table S8):

- mid October of 2019 (<Q2, rain-driven event)
- mid March 2021 (<Q2, snow-melt driven event)
- late-April/early-May 2021 (<Q2, rain-driven event)

Note that the gauging record for Lewis Creek at North Ferrisburg will not directly reflect magnitude, timing, and duration of peak flows that resulted in flood pulses at the Prindle Brook site. This site is located on a tributary to the Lewis, with an upstream drainage area of 2.7 mi^2, whereas the Lewis Creek gauge measures discharge from a 77 mi^2 area. Differences in peak flood magnitude and timing between this site and the downstream gauge may also reflect differences in the distribution of rainfall or snow melt driving these flooding events.

Table S8. Summary of flood pulse events sampled during the study period at Lewis Creek site, Prindle Brook.

	Event Peak Stage at Site	Event Peak Discharge at Gauge		
		Lewis Creek at		
	Prindle Brook	N. Ferrisburg, VT		
Sampled	TNC	Stn #04282780		Corresponding
Flood	Charlotte, VT	Instantaneous		Daily Mean
Pulse		Discharge		Discharge
Event	Date	(cfs)	Date Time	(cfs)
October 2019	10/18/2019	1080	10/18/2019 7:45	800
March 2021	3/12/2021	571 **	3/12/2021 16:00	436
April/May 2021	5/1/2021	1270 *	5/1/2021 7:30	925

* Discharge value, provisional.

** Discharge value, provisional, and gauge affected by ice.

Otter Creek sites – Union Street and Swamp Road

Recorded flood pulses at the Union Street and Swamp Road sites represented overbank flows sourced from the Otter Creek, and in the case of Union Street also reflected surface flows sourced from the Neshobe River tributary and local road drainage. Flood pulse events at the Otter Creek sites were identified with reference to sensor data (Table S9). Events were referenced to Daily Mean Flow (DMF) records at the upstream USGS gauge (Center Rutland)

and downstream USGS gauge (Middlebury). Note that gauging records in Center Rutland and Middlebury will not directly reflect magnitude, timing, and duration of peak flows that resulted in inundation at the Union Street and Swamp Road sites. This may be due to a difference in site elevations relative to the river (degree of vertical separation between the channel and the floodplain) and the setting of the Union Street site at the confluence of a tributary. Differences in inundation frequencies between the two Otter Creek sites may also reflect differences in distribution of rainfall or snow melt driving these flooding events, as well as longitudinal patterns in attenuation of flood waves between the sites.

- 10 events were captured by pressure transducers at the two sites during the study period
    - At the Otter Creek Center Rutland gauge, the lowest of the daily mean discharges corresponding to the inundation events recorded at Union Street and Swamp Road was 2120 cfs (60 cms), between a Qp99 and Qp95 event (Figure S18), where Qp99 is the 99th percentile of daily mean discharge estimated over the 29-year record, or that discharge value that is equaled or exceeded only 1% of the time.
    - At the Otter Creek Middlebury gauge, the lowest of the daily mean discharges corresponding to the inundation events recorded at the two sites was 2230 cfs (63 cms), between a Qp75 and Qp90 event (Figure S18).
- Multiple inundation events were recorded in each calendar year (2019, 2020, 2021).
    - All but one of the recorded inundation events at these sites were referenced to peak discharge values at the gauges lesser in magnitude than an AEP 50% event (2-year Recurrence Interval). The December 2020 event corresponded to an approximate AEP 50% event at the Otter Creek Center Rutland gauge (Table S7, HEC-SSP estimates).
- At least 8 of 10 events were co-occurring at the two sites. Note that some gaps in the record exist due to equipment malfunction and it is possible that events occurred and were not recorded.
    - Lag time between peak inundation at the two sites ranged from several hours to a few days. This finding reflects the possible event-scale variations in rainfall intensity and distribution and/or floodwater routing through the channel and floodplain attenuation, as well as differences in hydrograph character between Rutland (flashy) and Middlebury (gradual, broad peak).
- 3 events were sampled for water quality parameters (Table S9):
    - mid October 2019 (<Q2) – the same regional rain-driven event was sampled at the Lewis Creek Prindle Brook site
    - late December 2020 (~Q2 at Center Rutland gauge, snowmelt and rain-driven event)
    - late March 2021 (<Q2, rain-driven and mountain snowmelt event)

Table S9. Summary of flood pulse events observed during the study period at Otter Creek sites, Union Street and Swamp Road.

	Event Peak Stage at Site		Event Peak Discharge at Gage			
	Otter Creek **Union Street** NRCS	Otter Creek **Swamp Road** TNC	Otter Creek at Rutland, VT Stn #04282000		Otter Creek at Middlebury, VT Stn #04282500	
Flood Pulse Event	Brandon, VT Date	Salisbury, VT Date	Instantaneous Discharge (cfs)	Date Time	Instantaneous Discharge (cfs)	Date Time
May 2019	5/23/2019	5/26/2019	2730	5/20/2019 22:45	2770	5/20/2019 13:45
June 2019	6/23/2019	6/23/2019	3220	6/20/2019 23:00	2880	6/21/2019 2:45
Oct 2019	10/20/2019	10/21/2019	4200	10/17/2019 18:45	2600	10/18/2019 1:00
Nov 2019	11/4/2019	11/7/2019	3390	11/1/2019 10:30	2960	11/1/2019 12:00
Dec 2019	12/17/2019	No data	2190	12/15/2019 4:45	2390	12/18/2019 20:15
March 2020	3/16/2020	No data	2580	3/13/2020 21:15	2215	3/13/2020 22:15
April 2020	4/16/2020	4/20/2020	3320	4/14/2020 4:00	2610	4/14/2020 4:00
Dec 2020	12/28/2020	12/31/2020	5240	12/26/2020 8:45	1880	12/26/2020 2:00
March 2021	3/30/2021	4/3/2021	2840	3/26/2021 23:45	2790	4/4/2021 7:45
May 2021	5/3/2021	5/9-12/2021	3300	5/1/2021 16:30	2890	5/11/2021 10:00
		Average:	3301	(n = 10)	2673	(n = 8)
Corresponding Daily Mean Discharge (cfs)				Normalized by DA		Normalized by DA
Lowest Discharge (boxed values)			2120	6.9	2230	3.6
Average Discharge (shaded values)			3190	10.4	2780	4.4

Trend analysis

Using two different record lengths of daily mean discharge, we conducted a monotonic trend analysis for the number of days per year that discharge exceeded select threshold values. Threshold discharge values included the following percentiles calculated from the flow duration curves: Qp99, Qp95, Qp90, Qp75, and Qp50. Additionally, the lowest discharge and the average discharge corresponding to inundation events recorded at the Union Street and Swamp Road sites were also tested. Trend analysis was conducted in R using simple linear regression, following confirmation (using Shapiro Wilks test or visual inspection of Q-Q plots) that residuals followed a normal distribution (similar test outcomes were obtained using Mann-Kendall nonparametric trend tests).

Trend analysis for water years 1991 through 2019

Using the daily mean flow record at each of the USGS streamflow gaging stations, threshold discharge values above the Qp75 have not shown statistically significant increases in frequency over the most recent 29 years at any of the gages. Only the Qp75 and Qp50 discharges at the Center Rutland Otter Creek gage have occurred more frequently in the previous 29 years ($p < 0.05$) (Figure S23). A similar, though more modest increasing trend was noted for Qp75 and Qp50 discharges at the Otter Creek Middlebury and Lewis Creek gauges, but these trends were

not statistically significant (at $\alpha = 0.05$). Compared to water year 1991, Otter Creek near Center Rutland now experiences an additional 43 days per year on average at a discharge equal to or exceeding the 75th percentile (755 cfs, or 21 cms). However, this discharge does not appear to be great enough to result in inundation at either Union Street or Swamp Road.

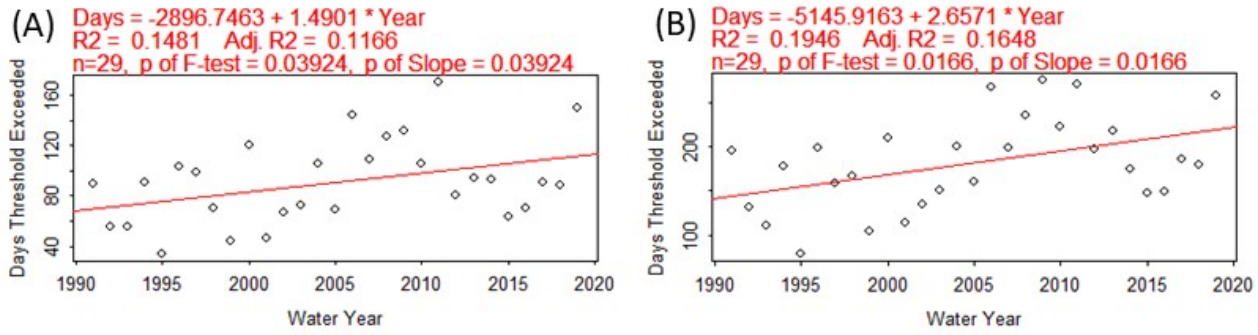

Figure S23. Number of days threshold exceeded regressed on water year for (A) Qp75 discharge threshold and (B) Qp50 discharge threshold at the USGS streamflow gauge at Otter Creek at Center Rutland for water years 1991 through 2019. Positive trends were statistically significant.

Trend analysis for water years 1931 through 2020 (Otter Creek sites only)

Monotonic trend analysis over the previous 90 years showed similar results to the trend analysis on the most recent 29-year record but yielded somewhat lower values for regression slopes (Table S10). Additionally, over this longer record, a statistically-significant, modestly increasing trend in the number of days exceeding the Qp99 threshold was detected for the Middlebury gauge. This finding is consistent with regional trends noted for minimally-disturbed catchments in New England states, where statistically-significant increasing trends in high-frequency flooding events (<Q5) have been observed associated with ~1970 timing of a phase change in the North Atlantic Oscillation (Collins, 2009; Armstrong, 2012).

Table S10. Summary of statistically significant monotonic trend results for water years 1931 through 2020 at Otter Creek stream gauging stations.

Gauge	Percentile	Threshold Discharge (cfs)	Trend	Regression Slope	Additional # of days on average exceeding threshold compared to 1931	Ordinary Linear Regression p value
Otter at Middlebury	Qp99	4210	Increasing	0.057	5	0.041
	Qp75	1650	Increasing	0.438	39	0.002
	Qp50	826	Increasing	0.859	77	1.68E-05
Otter at Center Rutland	Qp75	755	Increasing	0.363	32	0.002
	Qp50	421	Increasing	0.890	80	5.50E-06

REFERENCES

Armstrong WH, Collins MJ, and Snyder NP. 2012. Increased Frequency of Low-Magnitude Floods in New England. Journal of the American Water Resources Association 48(2):306-320. https://doi.org/10.1111/j.1752-1688.2011.00613.x

Bedford BL, Walbridge MR, & Aldous A. 1999. Patterns in Nutrient Availability and Plant Diversity of Temperate North American. Ecology 80(7):2151–2169. https://doi.org/10.2307/176900

Betts AK. 2011. Vermont Climate Change Indicators. Weather, Climate, and Society 3:106-115. doi: 10.1175/2011WCAS1096.1

Bolster CH, & Hornberger GM. 2007. On the Use of Linearized Langmuir Equations. Soil Science Society of America Journal 71(6):1796–1806. https://doi.org/10.2136/sssaj2006.0304

Bouyoucos GJ. 1962. Hydrometer method improved for making particle size analyses of soils. Agronomy 54(5):464–465.

Callaway, J. C., Cahoon, D. R., Lynch, J. C., DeLaune, R. D., Reddy, K. R., Richardson, C. J., & Megonigal, J. P. (2013). The Surface Elevation Table–Marker Horizon Method for Measuring Wetland Accretion and Elevation Dynamics. January. https://doi.org/10.2136/sssabookser10.c46

Chimney MJ, & Pietro KC. 2006. Decomposition of macrophyte litter in a subtropical constructed wetland in south Florida (USA). Ecological Engineering 27(4):301–321. https://doi.org/10.1016/j.ecoleng.2006.05.016

Cohn TA, Lane WL, and Baier WG. 1997. An algorithm for computing moments-based flood quantile estimates when historical flood information is available: Water Resources Research 33:2089–2096.

Cohn TA, Lane WL, and Stedinger JR. 2001. Confidence intervals for expected moments algorithm flood quantile estimates: Water Resources Research 37:1695–1706.

Cohn TA, England JF, Mason RR, Stedinger JR, & Lamontagne J. 2013. A Generalized Grubbs-Beck Test for Detecting Multiple Potentially Influential Low Outliers in Flood Series, Water Resources Research 49:5047-5058. https://doi.org/10.1002/wrcr.20392

Collins MJ. 2009. Evidence for Changing Flood Risk in New England Since the Late 20th Century. Journal of the American Water Resources Association 45(2):279-290. DOI: 10.1111/j.1752-1688.2008.00277.x

Cronk JK, & Fennessy MS. 2001. Wetland Plants: Biology and Ecology (1st ed.). CRC Press.

D'Angelo E, Crutchfield J, & Vandiviere M. 2001. Rapid, Sensitive, Microscale Determination of Phosphate in Water and Soil. Journal of Environment Quality 30:2206-2209. https://doi.org/10.2134/jeq2001.2206

Day PR. 1965. Hydrometer method of particle size analysis. Methods of soil analysis. Agronomy 9:562–566.

Diehl TH. 2008. A Modified Siphon Sampler for Shallow Water. Scientific Investigations Report 2007-5282. USGS. https://doi.org/10.3133/sir20075282

Dodds WK. 2003. The role of periphyton in phosphorus retention in shallow freshwater aquatic systems. J Phycol. 39(5):840–849. https://doi.org/10.1046/j.1529-8817.2003.02081.x

Dudley RW, Hodgkins GA, McHale MR, Kolian MJ, Renard B. 2017. Trends in snowmelt-related streamflow timing in the conterminous United States. J Hydrology 547:208-221.

Dunne EJ, Smith J, Perkins DB, Clark MW, Jawitz JW, & Reddy KR. 2007. Phosphorus storages in historically isolated wetland ecosystems and surrounding pasture uplands. Ecological Engineering, 31(1), 16–28. https://doi.org/10.1016/j.ecoleng.2007.05.004

England JF, Cohn TA, Faber BA, Stedinger JR, Thomas WO, Veilleux AG, et al. 2015. Guidelines for Determining Flood Flow Frequency, Bulletin 17C. Washington, D.C.: U.S. Department of the Interior.

Freeman C, Ostle N, & Kang H. 2001. An enzymic "latch" on a global carbon store. Nature 409(6817):149. https://doi.org/10.1038/35051650

Graetz DA, & Nair VD. 2009. Phosphorus Sorption Isotherm Determination. In G. M. Kovar, John L. Pierzynski (Ed.), Methods of Phosphorus Analysis for Soils, Sediments, Residuals, and Waters (2nd ed., pp. 33–38). Southern Cooperative Series Bulletin No. 408. http://www.sera17.ext.vt.edu/Documents/P_Methods2ndEdition2009.pdf

Guilbert J, Betts AK, Rizzo DM, Beckage B., and Bomblies A. 2015. Characterization of increased persistence and intensity of precipitation in the Northeastern United States. Geophys. Res. Lett. 42:1888–1893. https://doi.org/10.1002/2015GL063124.

Haan CT. 2002. Statistical Methods in Hydrology. 2nd ed. Ames, Iowa: Iowa State University Press.

Hantush MM, Kalin L, Isik S, & Yucekaya A. 2013. Nutrient Dynamics in Flooded Wetlands. I: Model Development. Journal of Hydrologic Engineering, 18(12), 1709–1723. https://doi.org/10.1061/(ASCE)HE.1943-5584.0000741

Hirsch RM, and Stedinger JR. 1987. Plotting positions for historical floods and their precision. Water Resour Res. 23(4):715– 727, doi:10.1029/WR023i004p00715.

Hodgkins GA, and Dudley RW. 2006. Changes in the timing of winter–spring streamflows in eastern North America, 1913–2002. Geophys. Res. Lett. 33:L06402, doi:10.1029/2005GL025593.

Hodgkins GA, & Dudley RW. 2011. Historical summer base flow and stormflow trends for New England rivers. Water Resources Research 47:W07528. https://doi.org/10.1029/2010WR009109.

Interagency Advisory Committee on Water Data. 1982. Guidelines for determining flood flow frequency: Bulletin 17B of the Hydrology Subcommittee; U.S. Department of the Interior, Geological Survey, Office of Water Data Coordination, Reston, Virginia, 183 p.

Jones, C. N., Scott, D. T., Guth, C., Hester, E. T., & Hession, W. C. 2015. Seasonal Variation in Floodplain Biogeochemical Processing in a Restored Headwater Stream. Environ Sci. and Techn, 49(22), 13190–13198. https://doi.org/10.1021/acs.est.5b02426

Lent RM, Weiskel PK, Lyford FP, Armstrong DS. 1997. Hydrologic indices for nontidal wetlands. Wetlands. 17(1):19-30. https://doi.org/10.1007/BF03160715

Levy ET, & Schlesinger WH. 1999. A comparison of fractionation methods for forms of phosphorus in soils. Biogeochemistry 47(1):25–38. https://doi.org/10.1007/bf00993095

Libohova Z, Seybold C, Wysocki D, Wills S, Schoeneberger P, Williams C, Lindbo D, Stott D, & Owens PR. 2018. Reevaluating the effects of soil organic matter and other properties on available water-holding capacity using the National Cooperative Soil Survey Characterization Database. J Soil Water Conserv. 73(4):411–421. https://doi.org/10.2489/jswc.73.4.411

Jarvie HP, Withers JA, Neal C. 2002. Review of robust measurement of phosphorus in river water: sampling, storage, fractionation and sensitivity. Hydrology and Earth System Science. 6(1):113-31. https://doi.org/10.5194/hess-6-113-2002

Marois, D. E., & Mitsch, W. J. 2016. Modeling phosphorus retention at low concentrations in Florida Everglades mesocosms. Ecological Modelling, 319, 42–62. https://doi.org/10.1016/j.ecolmodel.2015.09.024

McMillan, S. K., & Noe, G. B. 2017. Increasing floodplain connectivity through urban stream restoration increases nutrient and sediment retention. Ecological Engineering, 108 (March), 284–295. https://doi.org/10.1016/j.ecoleng.2017.08.006

Morris JT, Barber DC, Callaway JC, Chambers R, Hagen SC, Hopkinson CS, Johnson BJ, Megonigal P, Neubauer SC, Troxler T, & Wigand C. 2016. Contributions of organic and inorganic matter to sediment volume and accretion in tidal wetlands at steady state. Earth's Future 4(4):110–121.

Murphy J, & Riley JP. 1962. A modified single solution method for the determination of phosphate in natural waters. Analytica Chimica Acta 27(C):31–36. https://doi.org/10.1016/S0003-2670(00)88444-5

Nürnberg G, and Peters, RH. 1984. Biological Availability of Soluble Reactive Phosphorus in Anoxic and Oxic Freshwaters. Canadian Journal of Fisheries and Aquatic Sciences. 41(5): 757-765. https://doi.org/10.1139/f84-088

Nair VD, & Reddy KR. 2013. Phosphorus Sorption and Desorption in Wetland Soils. In SSSA Book Series SV - 10. Methods in Biogeochemistry of Wetlands (pp. 667–681). https://doi.org/10.2136/sssabookser10.c34

O'Dell JW. 1993. Method 365.1, Determination of Phosphorus by Semi-Automated Colorimetry. US EPA.

Olson SA. 2014. Estimation of flood discharges at selected annual exceedance probabilities for unregulated, rural streams in Vermont, with a section on Vermont regional skew regression, by Veilleux, A.G.: U.S. Geological Survey Scientific Investigations Report 2014-5078, 27 p. plus appendixes.

Patton CJ, & Kryskalla JR. 2003. Methods of Analysis by the U.S. Geological Survey National Water Quality Laboratory—Evaluation of Alkaline Persulfate Digestion as an Alternative to Kjeldahl Digestion for Determination of Total and Dissolved Nitrogen and Phosphorus in Water. In Water-Resources Investigations Report (Vols. 03–4174).

Reddy KR, & Delaune RD. 2008. Biogeochemistry of Wetlands: Science and Applications.

Reddy KR, Wang Y, DeBusk WF, Fisher MM, & Newman S. 1998. Forms of Soil Phosphorus in Selected Hydrologic Units of the Florida Everglades. Soil Science Society of America Journal 62(4):1134–1147. https://doi.org/10.2136/sssaj1998.03615995006200040039x

Richardson CJ, & Reddy KR. 2013. Methods for Soil Phosphorus Characterization and Analysis of Wetland Soils. In Methods in Biogeochemistry of Wetlands (pp. 603–638). Soil Science Society of America. https://doi.org/10.2136/sssabookser10.c32

Ringuet S, Sassano L, & Johnson ZI. 2011. A suite of microplate reader-based colorimetric methods to quantify ammonium, nitrate, orthophosphate and silicate concentrations for aquatic nutrient monitoring. J Environ Monit. 13(2):370–376. https://doi.org/10.1039/C0EM00290A

Roy ED, Nguyen NT, Bargu S, & White JR. 2012. Internal loading of phosphorus from sediments of Lake Pontchartrain (Louisiana, USA) with implications for eutrophication. Hydrobiologia 684(1):69–82. https://doi.org/10.1007/s10750-011-0969-9

Roy ED, Smith EA, Bargu S, & White JR. 2016. Will Mississippi River diversions designed for coastal restoration cause harmful algal blooms? Ecological Engineering 91:350–364. https://doi.org/10.1016/j.ecoleng.2016.02.030

Roy ED, Nguyen NT, & White JR. 2017. Changes in estuarine sediment phosphorus fractions during a large-scale Mississippi River diversion. Sci Total Environ. 609:1248–1257. https://doi.org/10.1016/j.scitotenv.2017.07.224

Ruttenberg KC. 2014. The Global Phosphorus Cycle. In Holland, HD, Turekian KK, editors. Treatise on Geochemistry: Second Edition, Vol. 10. Amsterdam: Elsevier Ltd. p. 499-558. https://doi.org/10.1016/B978-0-08-095975-7.00813-5Soil Science Division Staff. 2017. Soil Survey Manual, USDA Handbook 18. 18, 639.

Trentman MT, Tank JL, Jones SE, McMillan SK, Royer TV. 2020. Seasonal evaluation of biotic and abiotic factors suggests phosphorus retention in constructed floodplains in three agricultural streams. Sci Total Environ. 729: 138744. https://doi.org/10.1016/j.scitotenv.2020.138744

Trueheart ME, Dewoolkar MM, Rizzo DM, Huston D, Bomblies A. 2020. Simulating hydraulic interdependence between bridges along a river corridor under transient flood conditions. Sci Total Environ. 699: 134046. https://doi.org/10.1016/j.scitotenv.2019.134046

U.S. Army Corp of Engineers. 2019. Hydrologic Engineering Center Statistical Software Package (HEC-SSP), User's Manual. Davis, CA: Institute for Water Resources, retrieved from: https://www.hec.usace.army.mil/software/hec-ssp/documentation/HEC-SSP_22_Users_Manual.pdf

USGS 2021. National Water Information System, http://waterdata.usgs.gov/vt/nwis/rt.

Wang H, Appan A, & Gulliver JS. 2003. Modeling of phosphorus dynamics in aquatic sediments: I - Model development. Water Research 37:3928-3938. https://doi.org/10.1016/S0043-1354(03)00304-X

Watson K, Ricketts T, Galford G, Polasky S, O'Neill-Dunne J. 2016. Quantifying flood mitigation services: The economic value of Otter Creek wetlands and floodplains to Middlebury, VT. Ecological Economics 130:16-24.

Wiegman ARH, Myers GH, Augustin IC, Kubow ML, Fein-Cole MJ, Perillo VP, Ross DS, Diehl RM, Underwood KL, Bowden WB, and Roy ED. 2022. Potential for soil legacy phosphorus release from restored riparian wetlands within an agricultural landscape. Biogeochemistry 161:137-156.